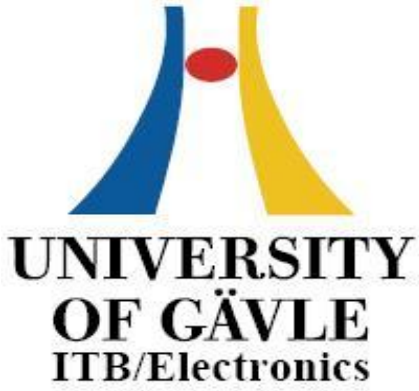

DEPARTMENT OF TECHNOLOGY AND BUILT ENVIRONMENT

THE STUDY AND IMPLEMENTATION OF MEANDER-LINE ANTENNA FOR AN INTEGRATED TRANSCEIVER DESIGN

MinJie Ma

Kai Deng

February-2010

Master Programme in Electronics/Telecommunications

Examiner:Prof.Claes Beckman

Supervisors:Prof.Bengt Oelmann,Peng Cheng(M.S.U)

Acknowledgments:

This master thesis has been performed at University of Gävle since 2009.5. The project is brought up and supported by Mid Sweden University.

We would like to show gratitude to our supervisor Prof. Claes Beckman for the opportunity of this thesis project which has been both interesting and challenging. Thank you for your kind help.

We also want to express our thanks to Prof. Bengt Oelmann and Peng Cheng, who give us this opportunity.

To all of our teachers and the staff at HIG we would like to forward deep thank for their great help.

The last gratitude and love are given to our parents who continuously support us to study abroad and encourage us during our living period in Sweden.

Abstract

This thesis focuses on the design and evaluation of the meander-line antenna geometry. One standard meander-line antenna and other two non-standard meander antennas have been studied. These printed antennas are discussed with the goal of identifying which is suitable for use in a miniaturized wireless transceiver design and which is able to provide the better performance using minimal Printed Circuit Board (PCB) space. In a word, the main objective is to characterize tradeoffs and identify which antenna provides the best compromise among volume, bandwidth and efficiency.

The performance of each antenna is evaluated based on return loss, operational bandwidth, and radiation pattern characteristics. During our measurement, return loss is measured by reading the S11-port reflection coefficient on Vector Network Analyzer (VNA). This coefficient can be used to characterize how well the antenna is able to be efficiently fed. Operational bandwidth is measured as the frequency range over which the antenna keeps the value of Voltage Standing Wave Ratio (VSWR) or equivalently has -10dB return loss. Ansoft High Frequency Structure Simulator (HFSS) is used to simulate expected characteristics which are resonant frequency, bandwidth, VSWR, and radiation pattern. HFSS is used to provide a good guide for the antenna design before the actual prototype is manufactured. Simulated results are compared with results of measurement to point out the differences and help demonstrate the practical effects on antenna performance. Radiation pattern are measured to illustrate the effects of antenna miniaturization. All the above measurements are done in the anechoic chamber.

Key Words: MLA GCPW PCB BALUN VNA

CONTENTS

CHAPTER 1

INTRODUCTION

1.1 Introduction

It is indisputable that antenna plays a significant part in communication system. Therefore, an increasingly number of technicians begin to do some research and development of antenna. However, with rapid development of the communication industry, the requirement of antenna will be achieved with high quality. Nowadays, there are different kinds of antennas in the market such as dipole antenna, patch antenna, loop antenna, meander-line antenna and so on. In order to meet the demand of developing communication equipment the research of antennas focuses on some particular aspect, for instance, how to reduce the size of antennas while maintaining higher radiation efficiency. Meanwhile, with the improvement of Small Scale Integrated circuits, the size of communications equipment is also getting smaller and smaller. Clearly compared with communication equipment, the dimension of antenna is too large. Therefore, the reduction of antenna size will be our research topic. In our thesis, we are trying to find a good antenna design solution on the reduction of the antenna size while maintaining higher efficiency.

1.2 Background

Radio Frequency Identification (RFID) of objects or people have become very popular in many services industry, distribution logistics, manufacturing companies and goods flow systems [1]. In all these applications data are transferred to a local querying system from a remote transponder including an antenna and a microchip transmitter, a suitable antenna for this remote transponder must have low-profile, low-cost and small-size and the bandwidth requirement is less important [2].

It is well known that the printed antenna is very mature in certain frequency such as GSM-900MHz DCS-1800MHZ and ISM-2400MHz. Printed antenna includes many advantages and attractiveness. It is easy to fabricate, low-cost and small-volume, In

order to work on Small Scale Integrated circuit board, designing a small size antenna is necessary.

The microstrip patch antenna is not suited. Base on G.A.Mavridis research, the miniaturized meander microstrip patch antenna was designed. The dimension of antenna with 36*44*0.75mm and antenna operating at 435MHz is designed on the Rogers RO3003 laminate substrate with ε_r=3.One study shows that the current on the surface of the patch is forced to follow a mender route [3]. Thus we increase the electrical length and the antenna's electrical size decreases. However, it does not improve the radiation efficiency of antenna because of low profile. The research solved the problem of the size of antenna, but it didn't take too much consideration of the radiation efficiency of antenna. S.VILLERS investigates how to reduce size of patch antenna for 400MHz. The research applied techniques of reduction of dimensions [4], [5] by achieving slots to the non-radiating edges and by introducing short-circuit points between the patch and the mass. In this way the total size of antenna is 91*66mm and the research reduces the dimensions of a factor 3, [6] but it is not enough.

Next, we consider the planar folded dipole antenna. This kind of antenna requires about 0.5 λ_0 length generally for obtaining a good performance [7]. Therefore, the size of folded dipole antenna is larger than the microstrip meander antenna because of monopole antenna has a mirror ground [8] [9].

In our case, for the purpose of reducing the size of transponder, a meander-line antenna (MLA) is an attractive choice. As proposed in [10] and discussed in [11], this class of antennas provides the largest size reduction at a given frequency at the expense of a narrow bandwidth. Compared with the PIFA antenna, there is an advantage that the MLA is relatively easy to catch larger relative bandwidth [12]. Also, according to [14] the table 1.1.1 shows that the monopole antenna is our best choice.

Meander-line antenna is a truly transformation of Monopole antenna. Therefore, in our work, we make a study on the meander-line antenna.

Antenna Type	Applications and Interest	Efficiency	Sensitivity to Detuning
Dipole	Large wire antenna; balanced feed	High	Moderate
Monopole	Large wire antenna; single-ended feed	High	Moderate
Loaded stub	Small wire and PCB antennas	Moderate	High
Transversal mode helical antenna	Small wire antennas	Moderate	High
Small loop	Body-wom antennas	Low	Low

Table 1.1.1: Features of Short Range Antennas [14]

1.3 Objectives

The coupling element and meander line antenna affect size of antenna and radiation efficiency in antenna structure, it has been introduced in background [3][6]. Thus coupling element and mender liner antenna will be studied.

The primary goal of this project is to design an antenna which operates at 433MHz with higher radiation efficiency and smaller size for the use in an integrated transceiver design. The entire design, including CC1101, balun, matching circuit and antenna, must fit on a single sided FR4 PCB (εr=4.4).All circuitry components including the transceiver chip, reference crystal and matching network must fit into the predefined ground plane area with dimensions of 40 mm length, 30 mm width and 1.2 mm thickness.

We design three kind of meander-line antenna. In order to evaluate the performance in a manner suitable for comparison, each antenna is identically implemented using a 50-Ohm Grounded Coplanar Waveguide (GCPW) as its feeding line. GCPW will allow each antenna to be independently assessed using a Vector Network Analyzer (VNA) for measurement of input-port reflection coefficient, efficiency and bandwidth.

Specialized equipment and an anechoic chamber will be used to measure antenna radiation patterns and characterize the antenna sensitivity to horizontally and vertically polarized data. The benefits and drawbacks will be shown in the last chapter and it will be demonstrated that there is no ideal antenna for each situation.

CHAPTER 2

ANTENNA THEORY

2.1 Basic definitions

Antenna Radiation Pattern is a plot of the radiation intensity in a determined plane. Two planes are mainly used here:

- Elevation plane: also called E-plane or θ-plane
- Azimuth plane: also called H-plane or φ-plane

Antenna Resistance is the total real valued resistance of the antenna.

Directivity is defined as the ratio of the radiation intensity in a given direction from the antenna to the radiation intensity averaged over all directions [20]. Also, it is a measure of how well the antenna radiates in a given direction respect to an isotropic antenna.

Efficiency is the ratio of the radiated power compared to the power available at the input of the antenna.

Gain is defined as the ratio of the power gain in a given direction to the power gain of a reference antenna in its referenced direction [20].

Input Impedance: the complex impedance of the antenna at its terminals which can be read on a Smith Chart with the real and imaginary parts.

VSWR is the Voltage Standing Wave Ratio defined as the ratio of reflected voltage to incident voltage in a standing wave pattern developed [20].

2.2 Meander-Line Antenna (MLA)

2.2.1 Introduction

The IEEE Standard Definitions of Terms for Antennas (IEEE Std 145-1983) defines the antenna as a metallic device for radiating or receiving radio waves [20] nowadays microstrip antennas are very popular, because they are low profile, inexpensive easy to fabricate by photolithographic processes. Microstrip antenna received considerable attention starting in the 1970s, although the idea of a microstrip antenna can be trace to 1953 and a patent in 1955 [20], the meander-line antenna is one type of microstrip antenna.

2.2.2 Principle

The meander-line antenna can be in a $\lambda/2$ dipole or $\lambda/4$ ground plane format. The idea is to fold the conductors back and forth to make the overall antenna shorter, which is shown in Figure 2.2.3. It is a smaller area, but the radiation resistance, efficiency and bandwidth decease [15]. The parameters of meander shape, for example H, La, Lb and Lc shown as in the figure will affect the antenna performance parameter [8]. In order to find the best antenna solution, different values of meander width are simulated and studied.

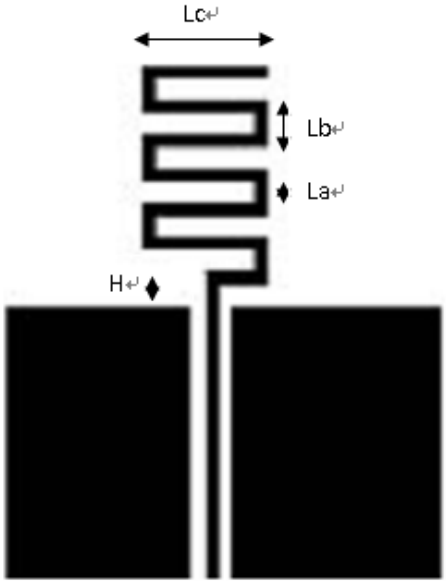

Figure 2.2.3 Shape of Meander Line Antenna (MLA)

A meander-line antenna can be realized by bending the conventional linear monopole antenna to decrease the size of antenna [16]. The influence of the meander part of the antenna is similar to a load and the meander line sections are considered as shorted-terminated transmission lines as shown in Figure 2.2.4. The meander line section can be modeled as an equivalent inductor. In the far-field pattern, in the result of the cancellation of magnetical fields, the transmission lines of a meander line antenna do not radiate fields. The radiation fields will be radiated from the vertical pars of MLA. The currents' intension of vertical parts can be clearly seen in Figure 2.2.5.

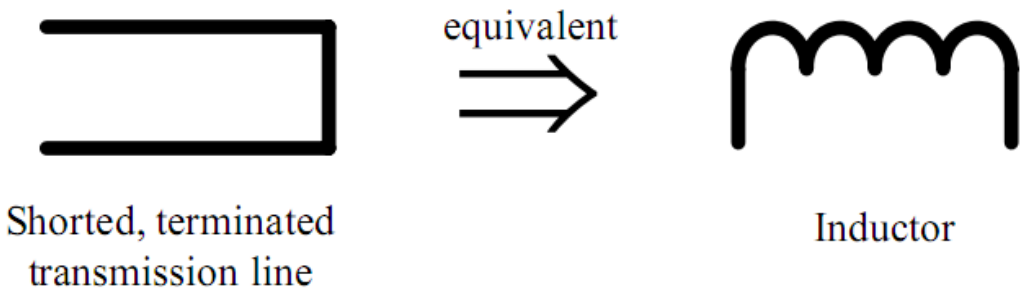

Figure 2.2.4: Equivalent Model of meander line sections [16]

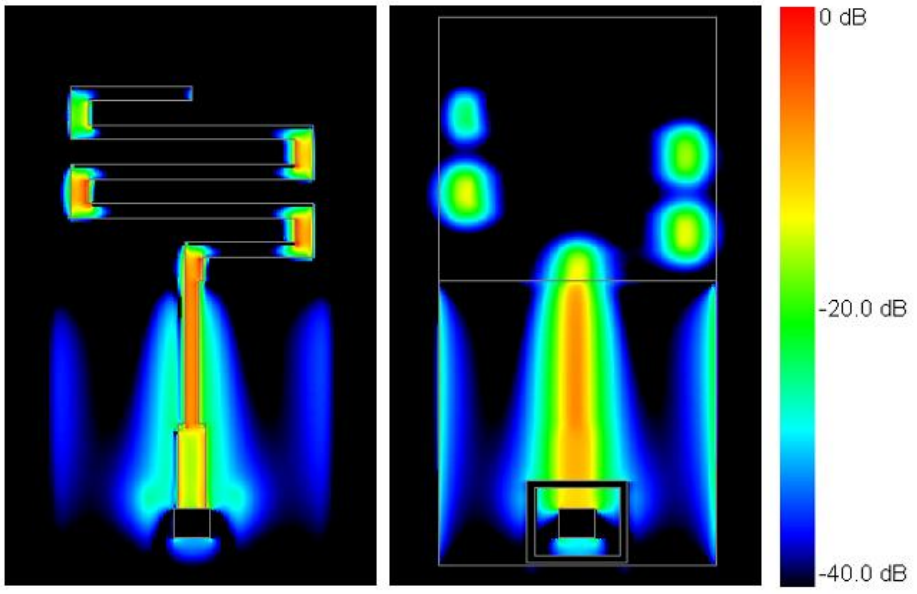

Figure 2.2.5: Electric Current Magnitude Plot for the MLA. Drawing on the left is the current on the upper traces. Drawing on the right is of the current on the groundplane. One can see that the large magnitude of the currents on the vertical sections of the meanderline. These are essentially the only sources of radiation when the groundplane is enlarged [17]

Different values of width (Lc) and width (La) are simulated as shown in table 1, and table 2 compared with figure 2.2.1 and 2.2.2. It is clearly known that when the length of width (Lc) and width (La) are larger, the resonant frequency will reduce quickly, and the shifted frequency is not linear.

Width Lc(mm)	Quantity						
	0	1	2	3	4	5	13
10	0.9557	0.909	0.8558	0.8381	0.8279	0.7874	0.6309
15	0.9557	0.8666	0.8001	0.7652	0.7316	0.6968	0.5029
19	0.9557	0.845	0.7646	0.7285	0.6791	0.6429	0.4491

Table 2.2.1 Different values of meander width (Lc)

Width La(mm)	Quantity							
	0	1	2	3	4	5	11	13
2	0.956	0.85	0.774	0.745	0.7	0.661	0.506	0.476
3	0.956	0.845	0.765	0.729	0.679	0.643	0.479	0.449
5	0.956	0.844	0.749	0.709	0.666	0.623	0.461	0.445-

Table 2.2.2 Different values of meander width (La)

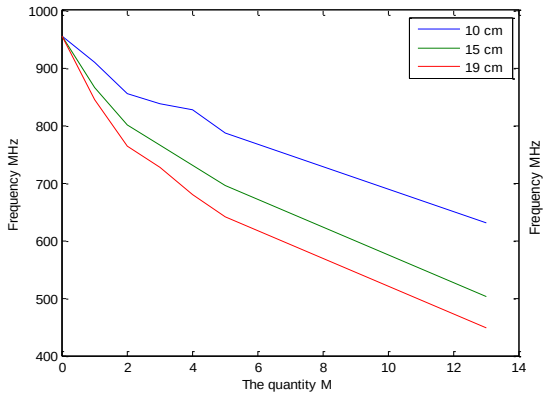

Fig 2.2.1 The length of Lc 10cm 15cm 19cm

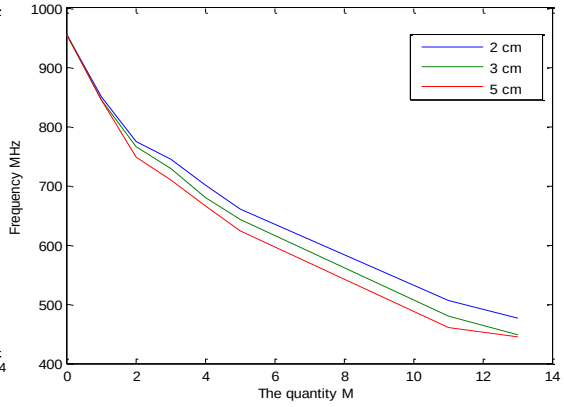

Fig 2.2.2 The length of La 2cm 3cm 5cm

We make three antenna designs. For different designs, they have different values for H and Lc.

The First Antenna Design: H =13 mm, Lc = 38 mm, La = 3 mm, Lb = 7 mm.

The Second Antenna Design: H = 5.5 mm, Lc = 36 mm, La = 3 mm, Lb = 7 mm.

The Third Antenna Design: H = 14 mm, Lc = 38 mm, La = 3 mm, Lb = 7 mm.

2.2.3 Performance

In our design, in order to obtain the amount of power radiated, a space which called keep-out zone has to be leave out. This concept is illustrated as Figure 2.2.5.

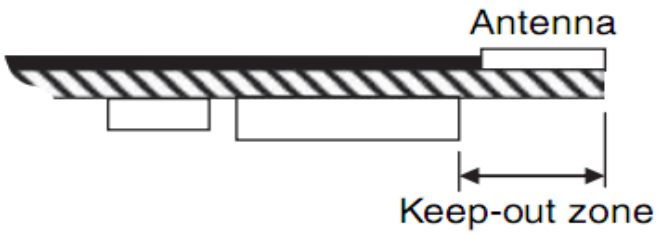

Figure 2.2.5 Antenna with a keepout zone which removes the ground plane [18]

We have established a set of goals for our specific antenna performance before our design procedure. In our project, we choose a fiberglass reinforced 1/2 oz copper-cladded FR4 epoxy with 1.2 mm thickness.

2.2.4 Grounded Coplanar Waveguide Feed

Nowadays Coplanar Waveguide transmission line is most popular. It own good characteristics such as low radiation loss, low dispersion, good control of characteristic impedance and uniplanar configuration and it is used in the field of integration of active solid-state devices with the antenna [19]. The Grounded Coplanar Waveguide (GCPW) geometry is shown as figure 2.2.6

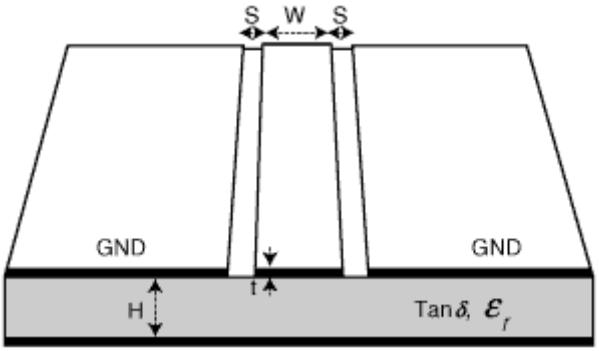

Figure 2.2.6 Ground Coplanar Waveguide geometry [13]

In this project, each antenna feed will be realized using a Grounded Coplanar Waveguide (GCPW) transmission line. GCPW geometry can be simulated by Advanced Design System (ADS) software. According to the ADS transmission line calculator, the dimension of GCPW can be shown as the figure 2.2.7 (W=2mm, G=1mm). We set the parameters as below:

PCB dielectric constant : $\varepsilon_r = 4.4$, Conductor thickness : T = 35 μm

Operating frequency : $f_0 = 433$ MHz , Substrate height : $H = 1.2$ mm

Characteristic impedance : $Z_0 = 50$ Ohm.

Under these settings, the groundplane seperation G = 1 mm and the conductor width W = 2 mm.

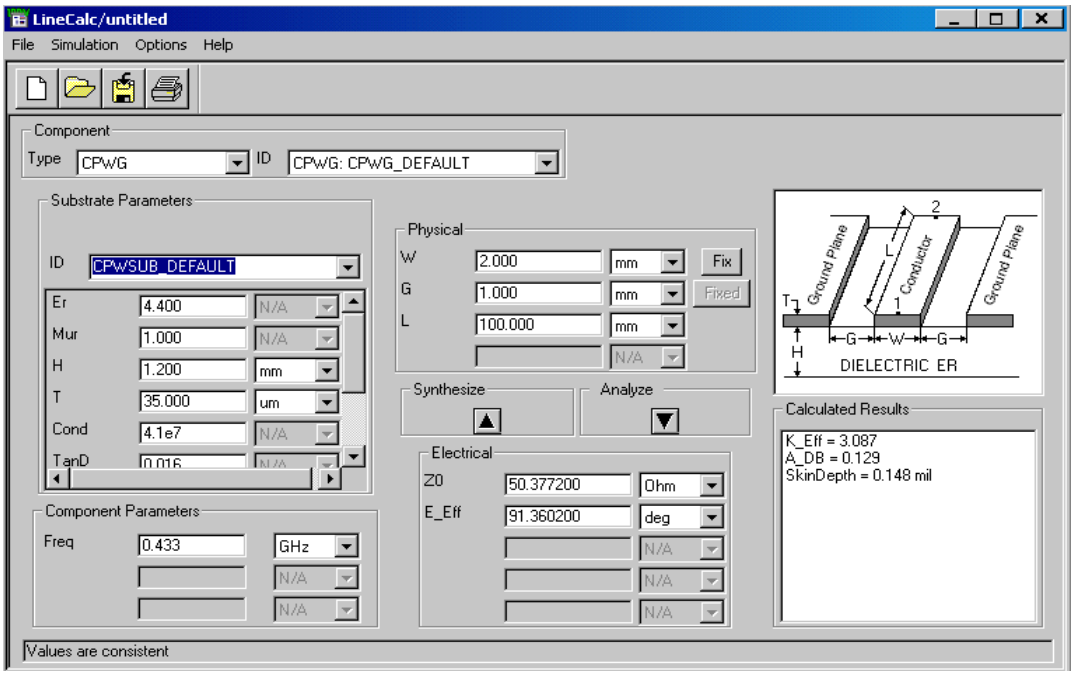

Figure 2.2.7: Line Calculator for GCPW.

2.2.5 Microstrip Width-to-Depth Ratio

The conductor width d, to substrate depth W, can be determined as the ratio W/d given a characteristic impedance Z_0 and substrate dielectric constant ε_r [20]. Following equations can be used to calculate microstrip width-to-depth ratio:

$$\frac{W}{d}=\begin{cases}\dfrac{8e^{A}}{e^{2A}-2} & (for\ W/d<2)\\ \dfrac{2}{\pi}[B-1-\ln(2B-1)+\dfrac{\varepsilon_r-1}{2\varepsilon_r}\left\{\text{`}\ln(B-1)+0.39-\dfrac{0.61}{\varepsilon_r}\right\}] & for\ W/d>2\end{cases}$$

Where,

$$A=\frac{Z_0}{60}\sqrt{\frac{\varepsilon_r+1}{2}}+\frac{\varepsilon_r-1}{\varepsilon_r+1}\left(0.23+\frac{0.11}{\varepsilon_r}\right)$$

$$B=\frac{377\pi}{2Z_0\sqrt{\varepsilon_r}}$$

In our project, the characteristic impedance of $Z_0=50$ ohms and FR4 dielectric constant $\varepsilon_r=4.4$, the resulting width-to-depth ratio is W/d =1.91. With a substrate thickness d=1.2 mm, the theoretically calculated microstrip width is W=2.3 mm. Compared with the LinCal of ADS, the value is almost the same.

CHAPTER 3

ANSOFT HFSS SIMULATION

The design is done with simulation Ansoft HFSS (High Frequency Structure Simulator) and PADS 2009 for 2D layout. It is used to simulate each antenna model including S11 reflection coefficients, radiation pattern, radiation efficiency and Voltage Standing Wave Ratio for studying characteristic parameter of antenna, the antenna designs, and measure results.

3.1 Matching network

For delivery maximum power, the impedance of the antenna connecting to the transmission line must be the same. There are matching network circuit and transmission line which can achieve the impedance to 50 ohms. In this project the matching circuit is used instead of transmission line, since transmission line take up much more space than matching circuit.

According to the Smith Chart, it is easily to match any impendence of antenna to 50 ohms, as shown in the figure 3.1.1 series or shunt capacitors and inductors could move the reflection coefficient on the circle. Using different values of the components on matching circuit, the reflection coefficient can be reached on the center of Smith Chart. [14]

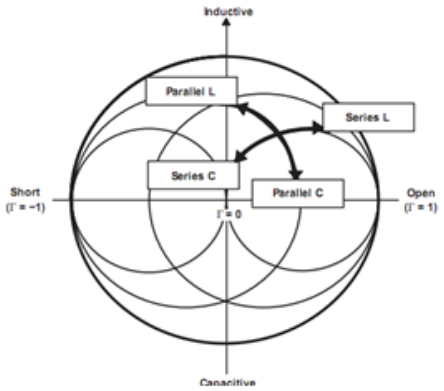

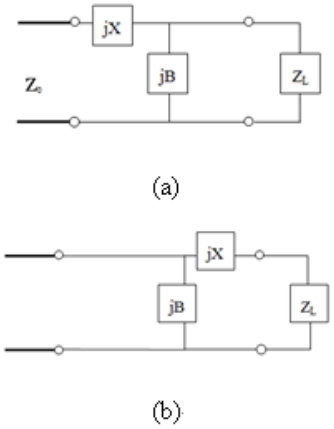

Fig 3.1.1 Smith Chart [14] **Fig 3.1.2 Matching network (a)** $R_L > Z_0$ **(b)** $R_L < Z_0$ **[13]**

From the figure3.1.2 (a) when the antenna impendence $R_L > Z_0$, equation 3.2 is a deduction from equation 3.1 and 3.2, it can get two solutions are possible for B and X, positive X means an inductor ,negative X means a capacitor, on the other hand while positive B means a capacitor negative B means an inductor. From the figure3.1.2 (b), when the antenna impendence $R_L < Z_0$ the arguments of the square root are always positive, again note that two solutions are possible. [13]

$$Z_0 = jx + \frac{1}{jB + 1/(R_L + JX_L)} \qquad 3.1$$

$$B = \frac{X_L \pm \sqrt{R_L / Z_0}\sqrt{R_L^2 + X_L^2 - Z_0 R_L}}{R_L^2 + X_L^2} \qquad 3.2$$

$$X = \frac{1}{B} + \frac{X_L Z_0}{R_L} - \frac{Z_0}{BR_L} \qquad 3.3$$

$$\frac{1}{Z_0} = jB + \frac{1}{R_L + j(X + JX_L)} \qquad 3.4$$

$$X = \pm\sqrt{R_L(Z_0 - R_L)} - X_L \qquad 3.5$$

$$B = \pm\frac{\sqrt{(Z_0 - R_L)/R_L}}{Z_0} \qquad 3.6$$

In the simulation, a 50 ohms lump-port is used. The 0402-size of Lump port-RLC is used to simulate the matching network in Ansoft HFSS. The frequency sweep is setup for a 433 MHz solution with a start at 350 MHz and ending at 550 MHz The far-field radiation pattern is simulated using a 35 cm * 35 cm *35 cm air box.

3.2 The first Meander-line Antenna Simulation

3.2.1 Antenna Orientation and Matching Circuit

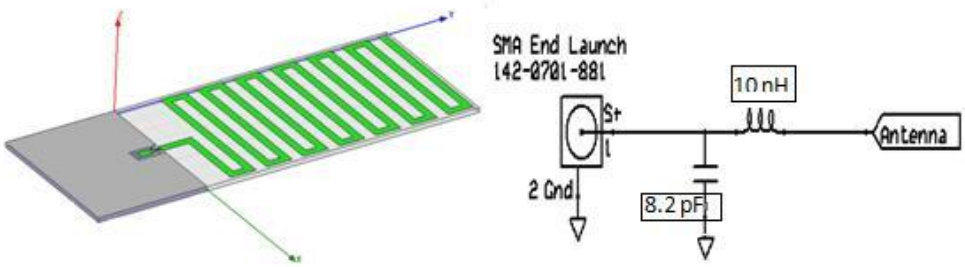

Figure 3.2.1: The first meander-line antenna orientation and simulated matching network required for 50-Ohm match.

3.2.2 Simulated 3D radiation pattern and 2D radiation pattern

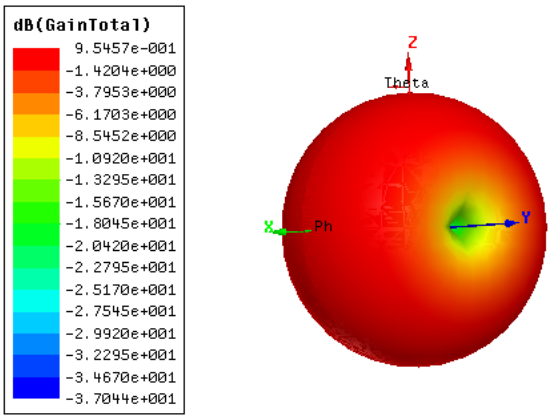

Figure 3.2.2: The first meander-line antenna simulated 3D-radiation pattern expressed as Gain in dB

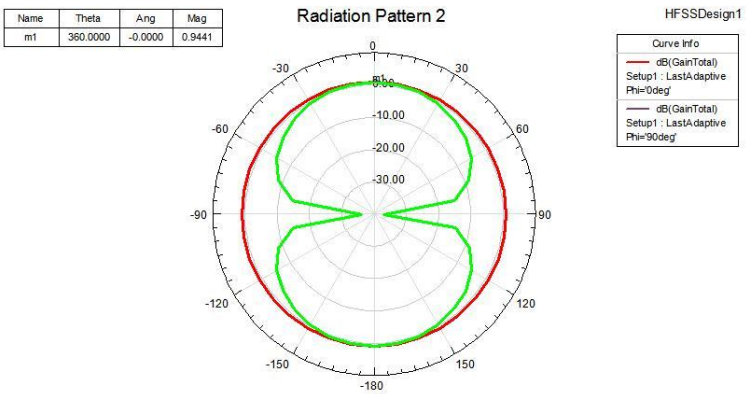

Figure 3.2.3: The first meander-line antenna simulated 2D-radiation pattern expressed as Gain in dB

3.2.3 Simulated S11 Reflection Coefficient (dB)

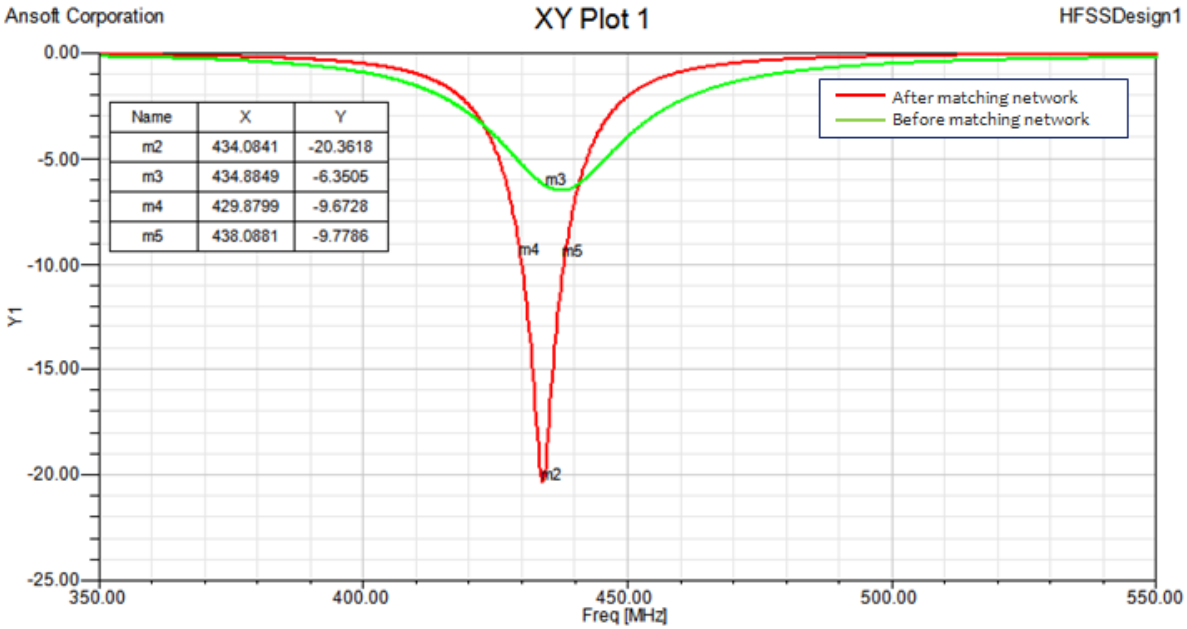

Figure 3.2.4: The first meander-line antenna input-port reflection coefficient expressed in dB before addition of a matching network and after addition of a matching network.

3.2.4 Simulated Smith Chart

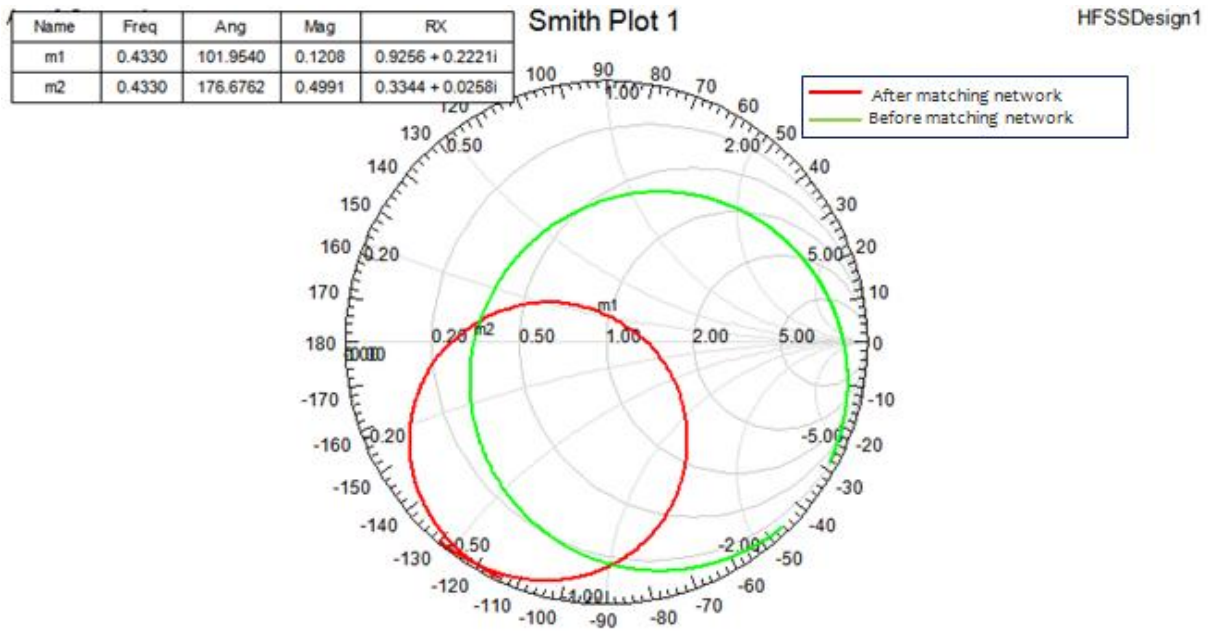

Figure 3.2.5: The first meander-line antenna's Smith Chart before addition of a matching network and after addition of a matching network.

3.2.5 Simulated Voltage Standing Wave Ratio (VSWR)

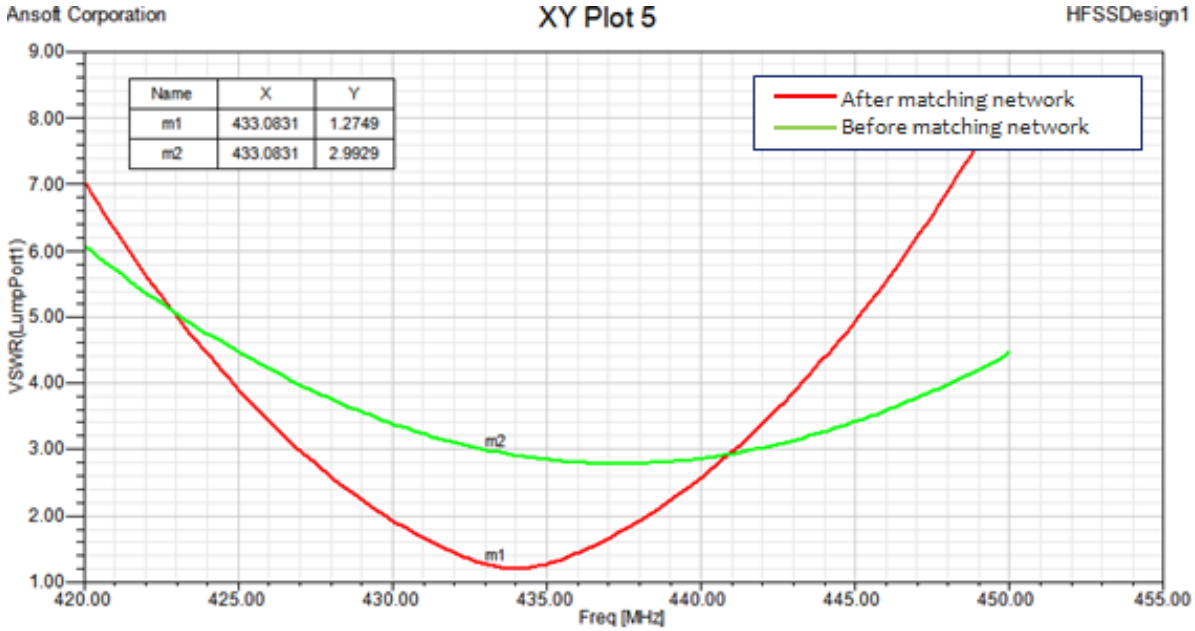

Figure 3.2.6: The first meander-line antenna input-port Voltage Standing Wave Ratio before addition of a matching network and after addition of a matching network.

3.2.6 Summary of the first time simulation

The first small size of meander-line antenna is designed. The meander-line antenna with dimension of 105mm*39mm*1.2mm, the substrate dielectric constant ε_r=4.4. Based on HFSS simulation it is shown that the S11 return loss is -6 dB at 433 MHz before addition of the matching network. After adding a series of 10 nH and a shunt of 8.2 pF, the return loss at 433 MHz can be lowered to -20 dB, the radiation efficiency of antenna is 92% and the VSWR bandwidth is almost 8 MHz. The expected peak gain is 0.95 dBi.

Clearly the radiation efficiency of the first meander-line antenna is achieved with demands, but the dimensions of antenna are far from satisfactory. Generally speaking, in order to improve the radiation efficiency of antenna, the total length of the antenna must increase which is the main reason why we have large dimension. For the improvement of the antenna size, in the next part the second meander line antenna is designed

3.3 The second meander-line antenna Simulation

3.3.1 Antenna orientation and Matching Circuit

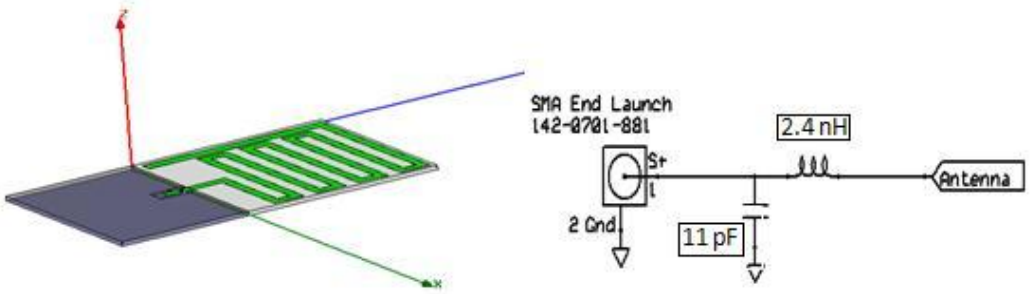

Figure 3.3.1: The second meander-line antenna orientation and simulated matching network required for 50-Ohm match.

3.3.2 Simulated 3D Radiation Pattern Gain and 2D Radiation Pattern Gain

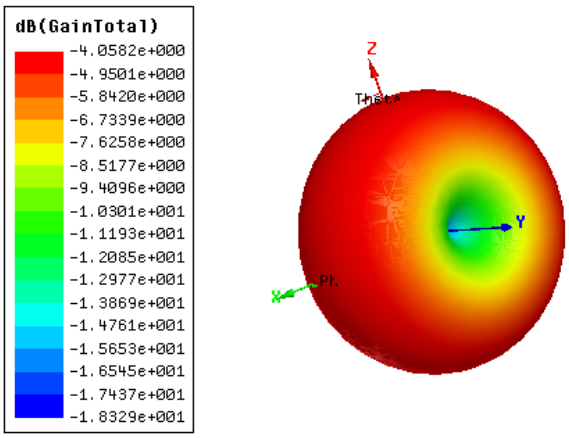

Figure 3.3.2: The second meander-line antenna simulated 3D-radiation pattern expressed as Gain in dB.

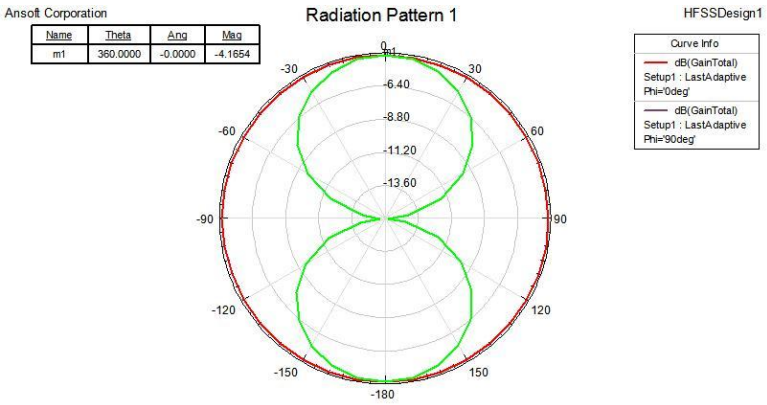

Figure 3.3.3: The second meander-line simulated 2D-radiation pattern expressed as Gain in dB.

3.3.3 Simulated S11 Reflection Coefficient (dB)

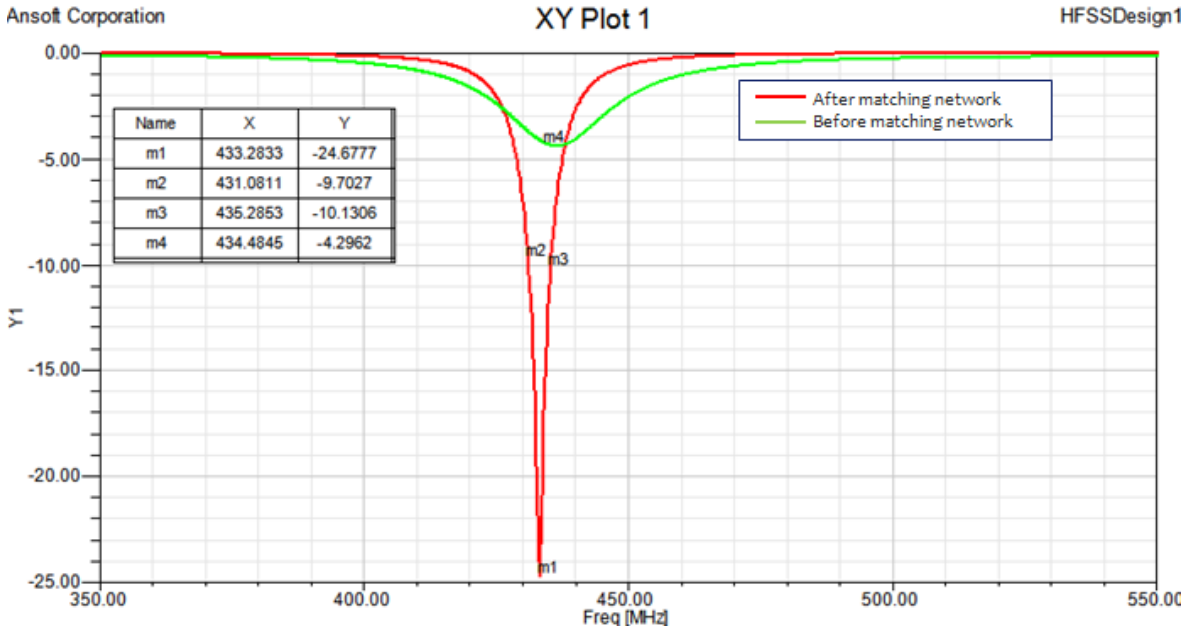

Figure 3.3.4: The second meander-line antenna input-port reflection coefficient expressed in dB before addition of a matching network and after addition of a matching network.

3.3.4 Simulated Smith Chart

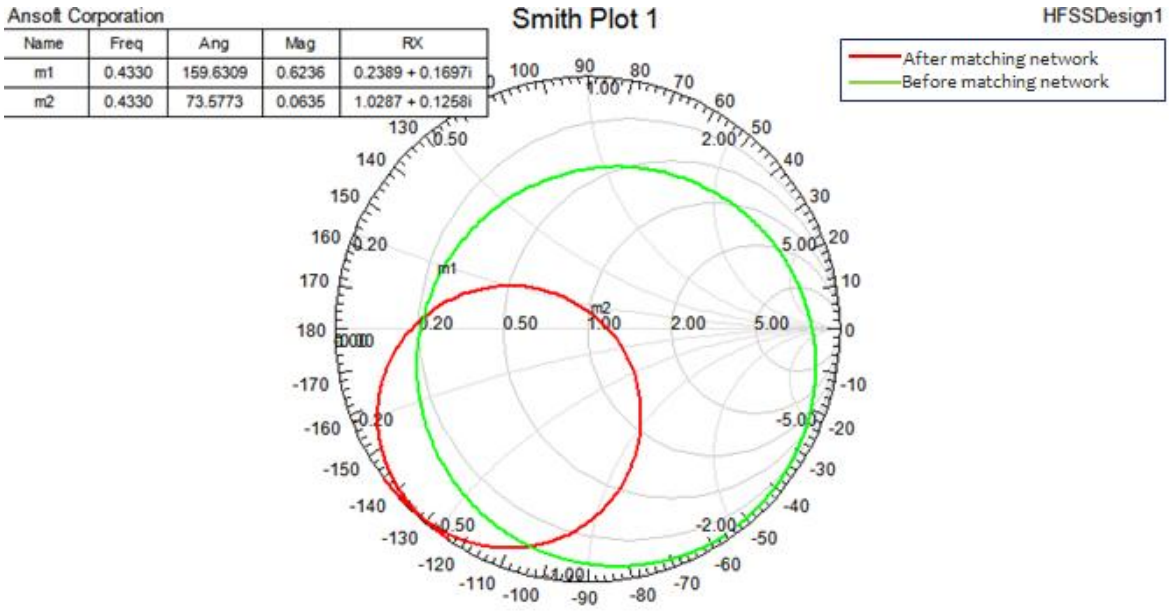

Figure 3.3.5: The second meander-line antenna's Smith Chart before addition of a matching network and after addition of a matching network.

3.3.5 Simulated Voltage Standing Wave Ratio (VSWR)

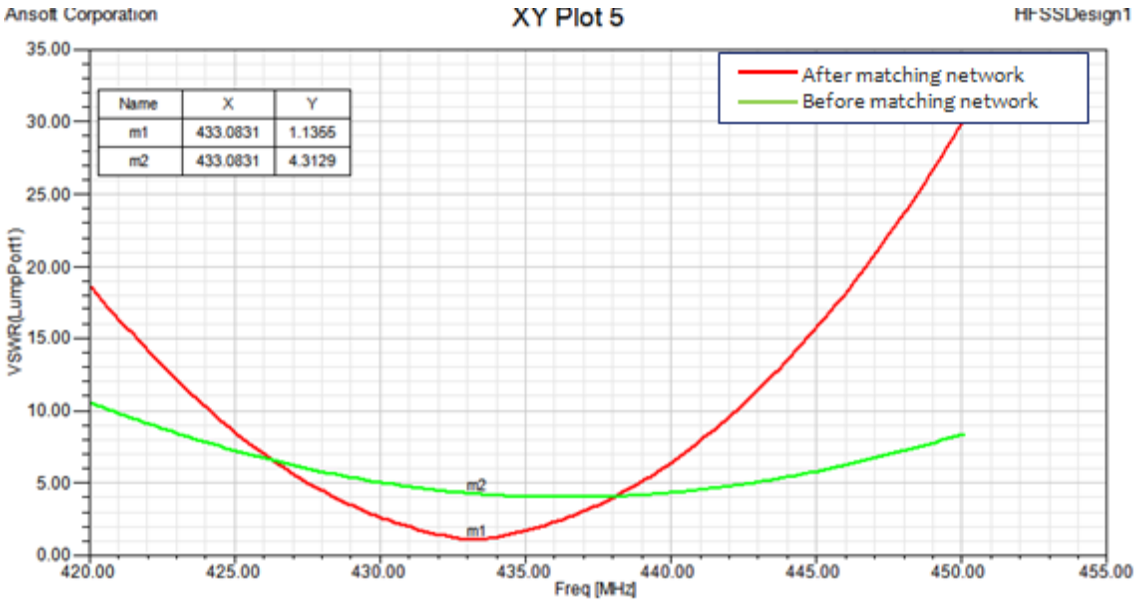

Figure 3.3.6: The second meander-line antenna input-port Voltage Standing Wave Ratio before addition of a matching network and after addition of a matching network.

3.3.6 Summary of the second time simulation

According to the second meander-line simulation, the dimension of the antenna is 75mm*39mm*1.2mm, the return loss is -4 dB which is not good. After addition of matching network (a series of 2.4 nH and a shunt of 11 pF), the return loss is -25 dB at 433MHz. The radiation efficiency of antenna is 39%The VSWR bandwidth is 5 MHz the expected peak gain is -4 dBi.

Obviously, increasing radiation part and decreasing electric length are used to improve the size of the antenna. The size of the antenna is quite satisfied with our requirement, but unfortunately, the efficiency of the antenna, the gain of the antenna and bandwidth is lower than the first meander line antenna. Just as chapter 1 mention that the size will affect efficiency, gain and bandwidth. Therefore, to combine experiences of first time and second time simulation new construction antenna must be considered in the next part.

3.4 The third meander-line antenna Simulation

3.4.1 Antenna Orientation and Matching Circuit

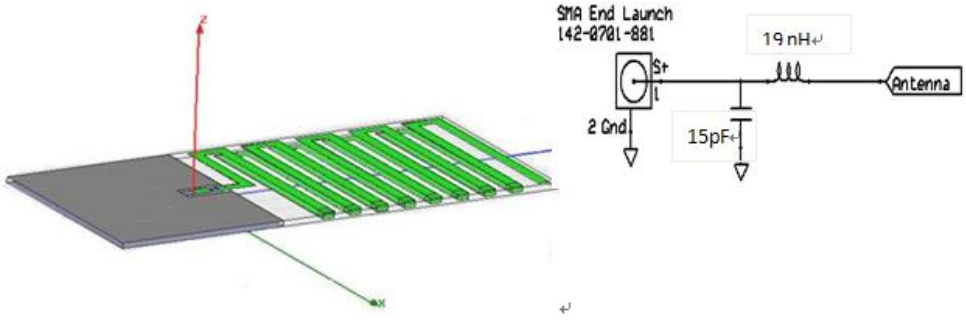

Figure 3.4.1: The third meander-line antenna orientation and simulated matching network required for 50-Ohm match.

3.4.2 Simulated 3D Radiation Pattern Gain and 2D Radiation Pattern Gain

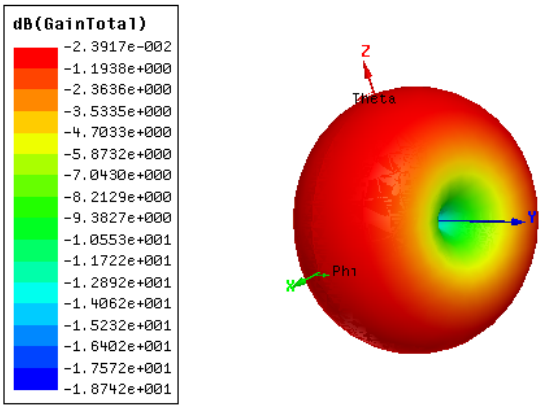

Figure 3.4.2: The third meander-line antenna simulated 3D-radiation pattern expressed as Gain in dB.

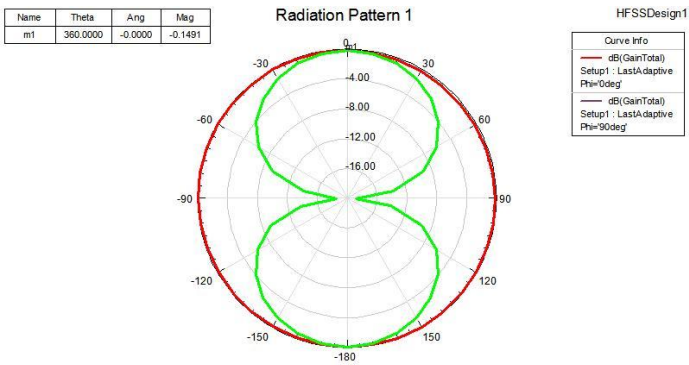

Figure 3.4.3: The third meander-line antenna simulated 2D-radiation pattern expressed as Gain in dB.

3.4.3 Simulated S11 Reflection Coefficient (dB)

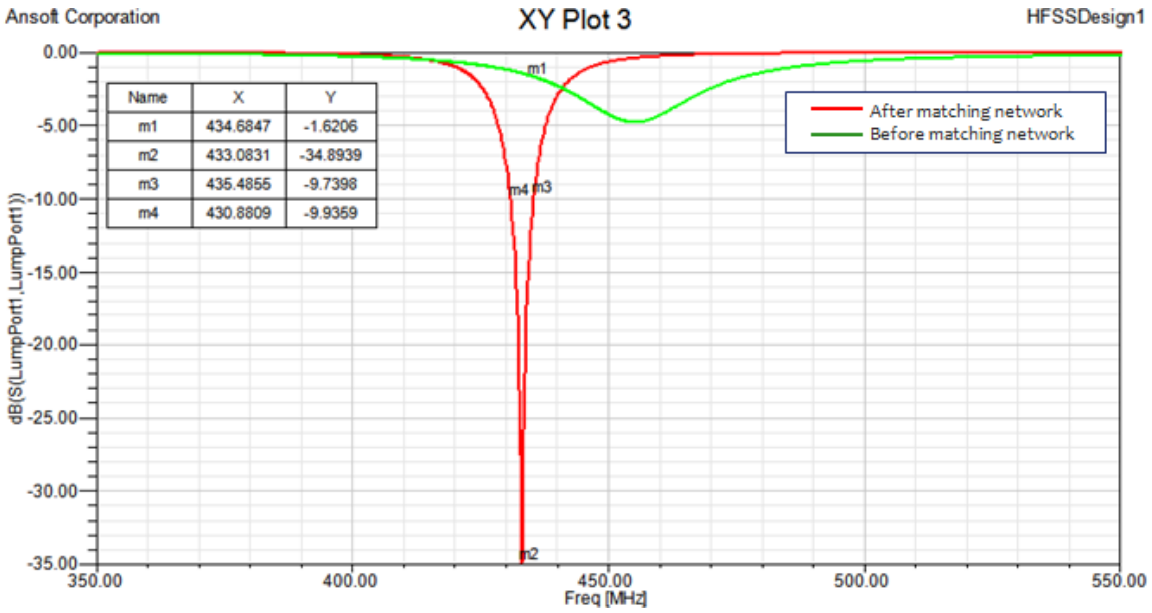

Figure 3.4.4: The third meander-line antenna input-port reflection coefficient expressed in dB before addition of a matching network and after addition of a matching network.

3.4.4 Simulated Smith Chart

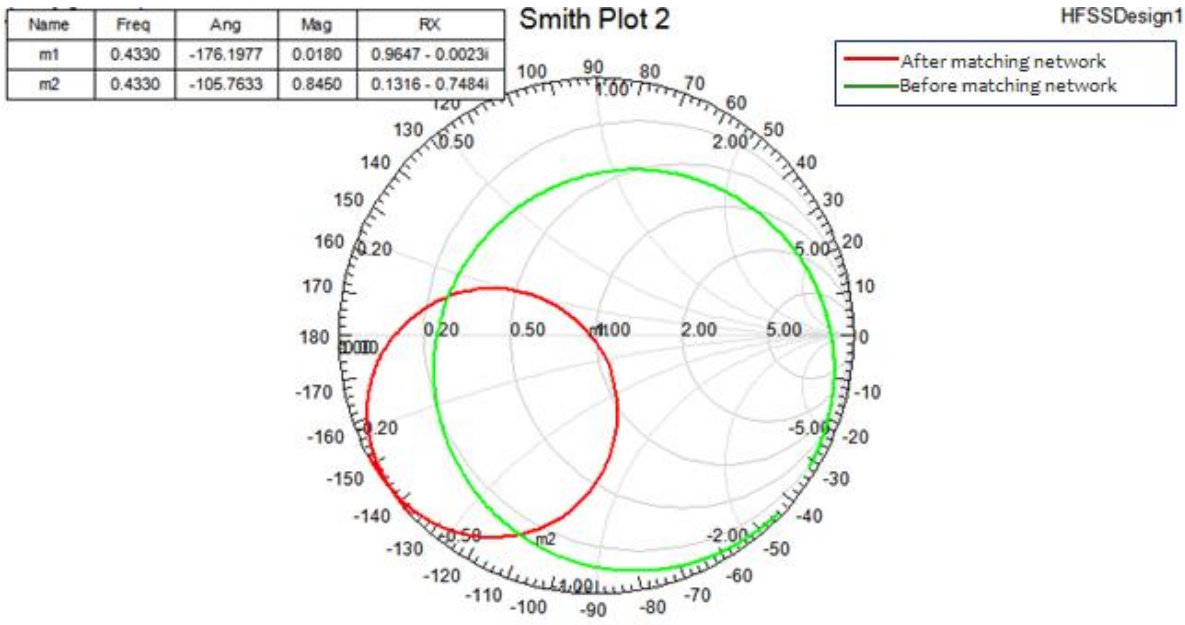

Figure 3.4.5: The third meander-line antenna Smith Chart before addition of a matching network and after addition of a matching network.

3.4.5 Simulated Voltage Standing Wave Ratio (VSWR)

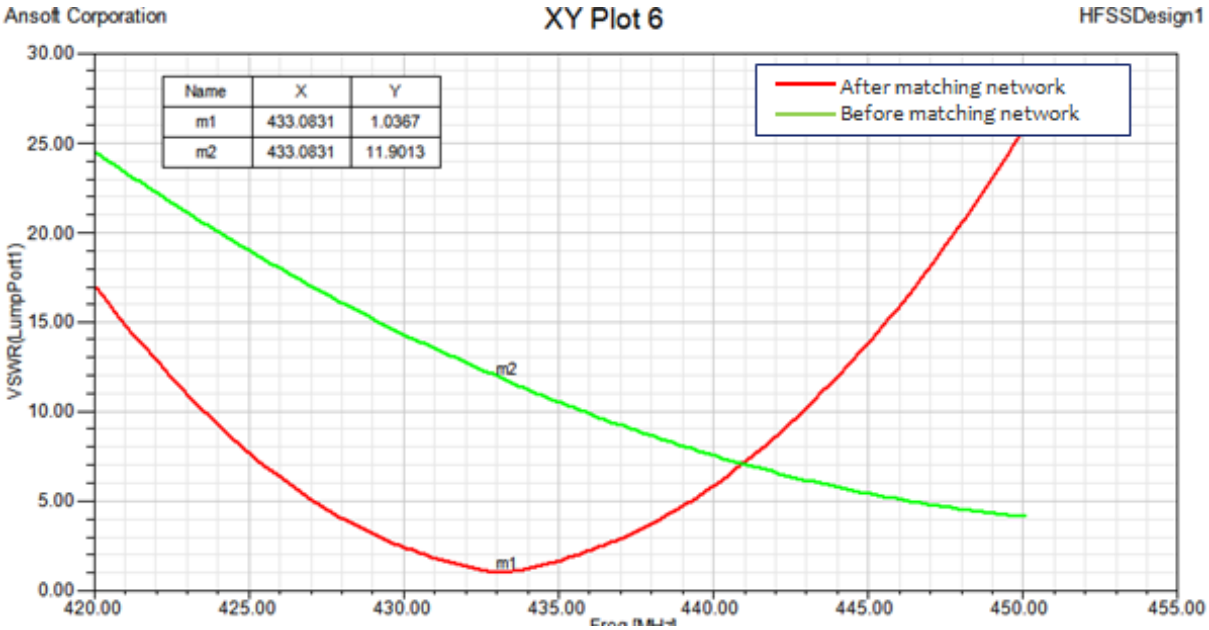

Figure 3.4.6: The third meander-line antenna input-port Voltage Standing Wave Ratio after addition of a matching network.

3.4.6 Summary of the third time simulation

A two-sided printed meander-line antenna is simulated in this part. The dimension of the antenna is 79mm*39mm*1.2mm.The simulated data shows that the return loss is -1.5 dB which is too bad. After adding a series of 19 nH and a shunt of 15 pF, the return loss is lowered to -35 dB at 433 MHz ,the radiation efficiency of antenna is 51%, the VSWR bandwidth is almost 5 MHz .The expected peak gain is -0.02 dBi. Compared with first type and second type antenna, the size of antenna and radiation efficiency are both satisfied with our requirements, simplify speaking the idea of the third time simulation are derived from the first time and second time simulation.

3.5 Ansoft Simulation Results

Based upon the simulated data, from the table 3.4.1, it can be shown that each antenna has the ability to be matched and will be resonated properly at 433 MHz From the simulated data, by miniaturizing the size of antennas, we can obtain a good performance especially from the third meander-line antenna at the resonant frequency

433 MHz.

Design	Bandwidth	Dimension	substrate	S11	Max Gain	Antenna efficiency
Board1	39 MHz	105mm*39mm*1.2mm	ε_r=4.4	-20.36	1.05	92%
Board2	30 MHz	75mm*39mm*1.2mm	ε_r=4.4	-24.67	-1.27	39%
Board3	5 MHz	79mm*39mm*1.2mm	ε_r=4.4	-34.8	-1.06	51%

Table 3.4.1 Comparison of test antenna S parameter

In our design, we are trying to make the VSWR under 2 which also means that at the resonant frequency the return loss (S11) will below -10 dB.

As a summary of the simulated data from these three antennas, the third antenna is the most expected one with a smaller size and better gain. In Chapter 5, we will make a measurement of all these three antenna prototypes. A comparison will also be provided in Chapter 5.

CHAPTER 4

ANTENNA MODEL AND MEASUREMENT METHOD

4.1 Antenna Model

In this section, all the PCB designs will have their layouts using PADS 9.0 software. Figure 4.1.1 shows the completed drawings of our antennas. Figure 4.1.2 shows the final designs of our antenna models.

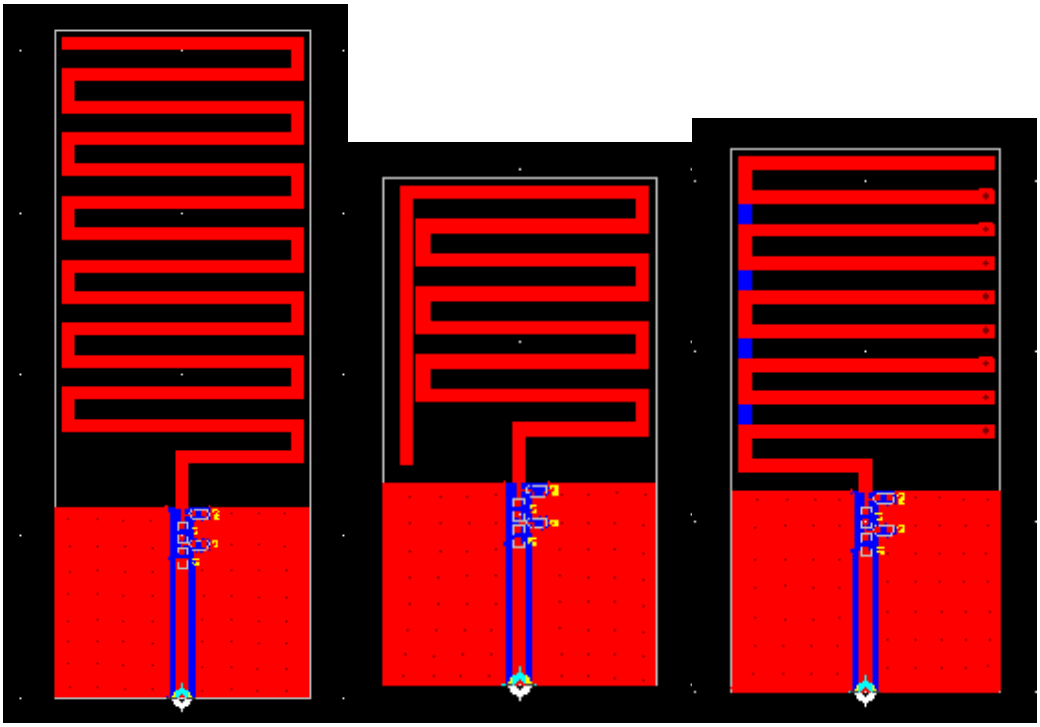

Figure 4.1.1: Completed Antenna Drafting Using PADS 9.0.

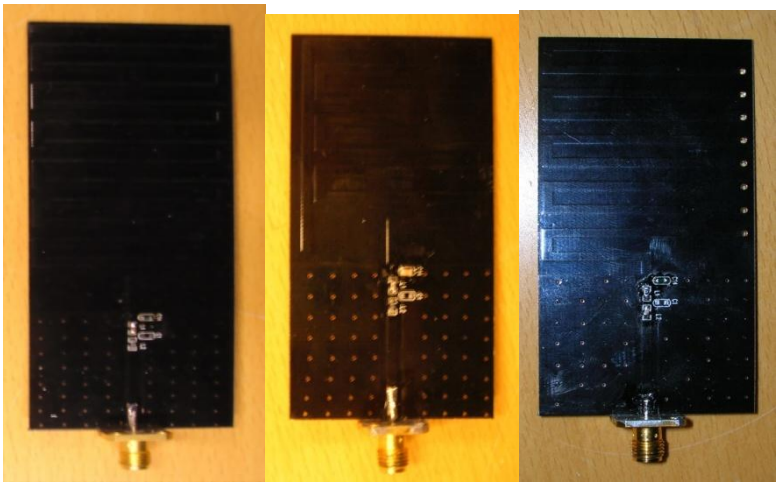

Figure 4.1.2: Completed Antenna Models.

4.2 Antenna S-Parameter Measurement

An HP 8753D Network Analyzer is used to measure certain transmission properties of antenna. The key step of measurement is calibration, to be able of exact measuring; the network analyzer is accomplished by performing a calibration. Measurement-S11 parameter is used to determine how much of the transmitted power can be reached at the ending of an antenna. This measurement gives us the evidence to build a proper matching network. During the whole process of measurement, prototypes are placed inside the anechoic chamber for measurement of S11 magnitude, Smith Chart and VSWR. All these data will be demonstrated clearly in Chapter 5.

Figure 4.2.1: HP 8753D Network Analyzer (30 kHz~6 GHz)

4.3 Antenna Radiation Pattern Measurement

This section introduces the method to measure the radiation pattern. This method is based on the friis formula [5]:

$$\frac{P_r}{P_t} = e_{cdt} e_{cdr} (1-|\Gamma_t|^2)(1-|\Gamma_r|^2)(\frac{\lambda}{4\pi R})^2 D_t(\theta_t,\phi_t) D(\theta_r,\phi_r) |\hat{\rho}_t \cdot \hat{\rho}_r|^2 \quad (4\text{-}1)$$

For reflection and polarization-matched antennas aligned for maximum directional radiation and reception, the formula reduces to

$$\frac{P_r}{P_t} = \left(\frac{\lambda}{4\pi R}\right)^2 G_{0t} G_{0r} \quad (4\text{-}2)$$

In our method, the two antennas are separated by a distance R, and must satisfy the far-field criterion of each antenna. The formula (4-2) can be written in a logarithmic decibel form as

$$(G_{0t})_{dB}+(G_{0r})_{dB}=20\log_{10}\left(\frac{4\pi R}{\lambda}\right)+10\log_{10}\left(\frac{P_r}{P_t}\right) \qquad (4\text{-}3)$$

In our measurement, the transmitting and receiving antennas are identical ($G_{0t}=G_{0r}$), (4-3) reduces to

$$(G_{0t})_{dB}=(G_{0r})_{dB}=\frac{1}{2}\left[20\log_{10}\left(\frac{4\pi R}{\lambda}\right)+10\log_{10}\left(\frac{P_r}{P_t}\right)\right] \qquad (4\text{-}4)$$

By measuring R, λ, and the ratio of P_r / P_t, the gain of the antenna can be found. At a given frequency, this can be accomplished using the system of Figure 4.3.1.

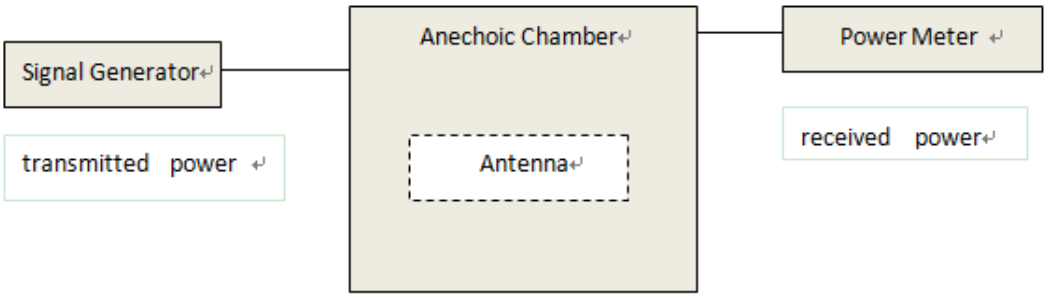

Figure 4.3.1 The Set-Up for measuring radiation pattern

Figure 4.3.2: Anechoic Chamber.

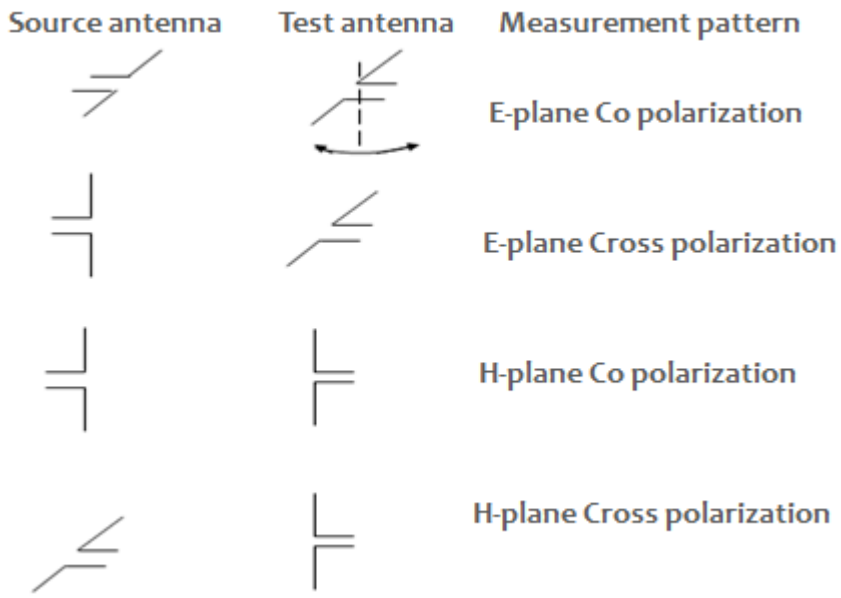

Fig 4.3.3 Measurement Method

In our lab, an anechoic chamber can be used to place the antenna. The anechoic chamber is shown in figure 4.3.2, in which the test antenna is rotated from 0 degree to 360 degree to measure radiation pattern under different plane and polarizations which are shown in figure 4.3.3. According to [20], the far-field range of an antenna is $R \geq 2D^2 / \lambda$. Here, R is the radius of the circle which made by the center of antenna. D is the antenna's maximum dimension. The finalized plots are presented in the measurement results Chapter 5.

CHAPTER 5

MEASUREMENT RESULTS

In this chapter, we do the S11 measurement after addition of our matching network. In the case of the real measurement, there are few differences between actual values of matching network and the simulated values. Return loss (S11), Smith Chart and VSWR after addition of matching network are measured using Network Analyzer. The radiation pattern is also measured using the last chapter's method. All these measurements are done with the antennas in the anechoic chamber.

5.1 The First Meander-Line Antenna

5.1.1 Antenna and Matching Network

The first meander-line antenna's prototype and its matching network are shown in Figure 5.1.1.

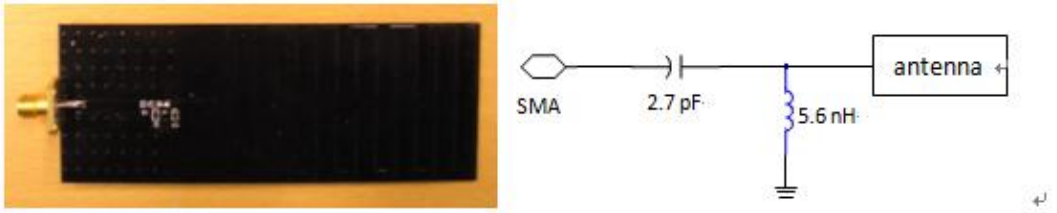

Figure 5.1.1: First meander-line antenna prototype and matching network.

5.1.2 S11 Reflection Coefficient after matching

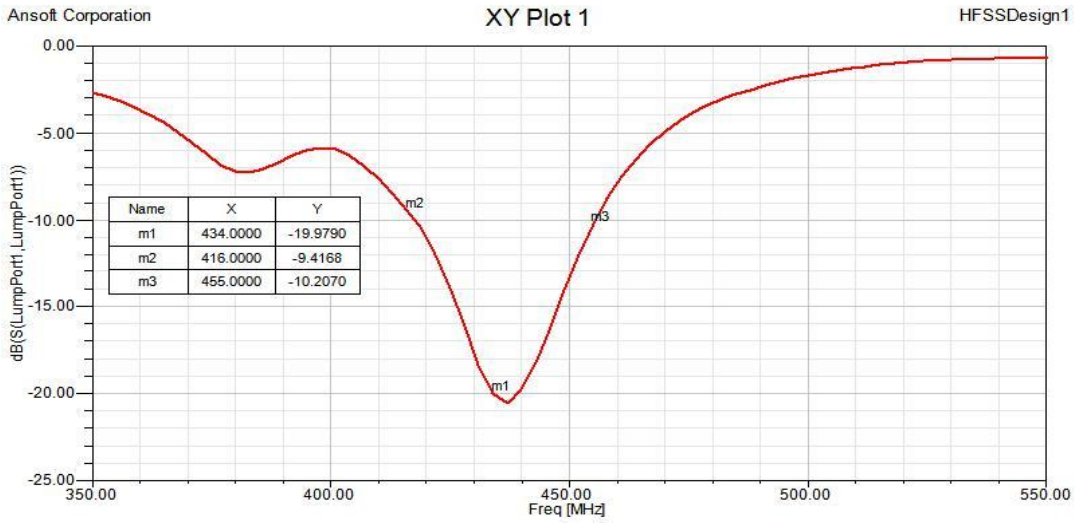

Figure 5.1.2: The first meander-line input-port reflection coefficient (S11) expressed in dB.

5.1.3 Simulated Smith Chart

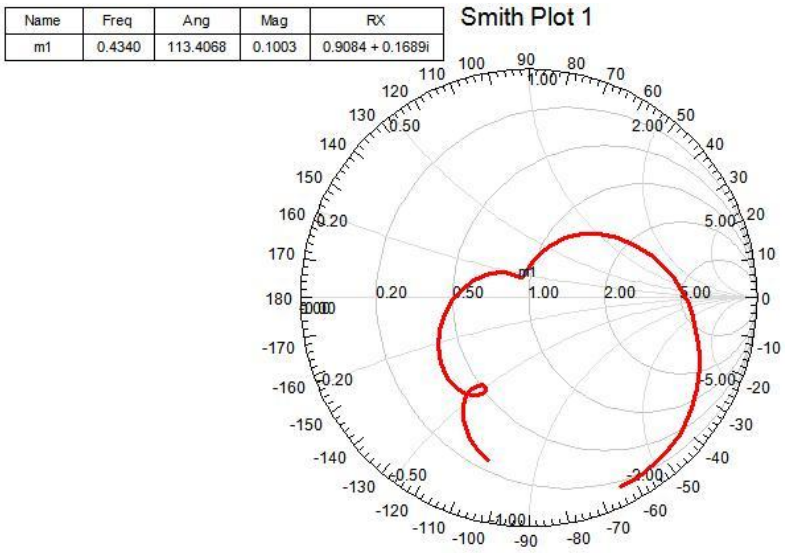

Figure 5.1.3: The first meander-line antenna input-port Smith Chart.

5.1.4 Voltage Standing Wave Ratio (VSWR) after matching

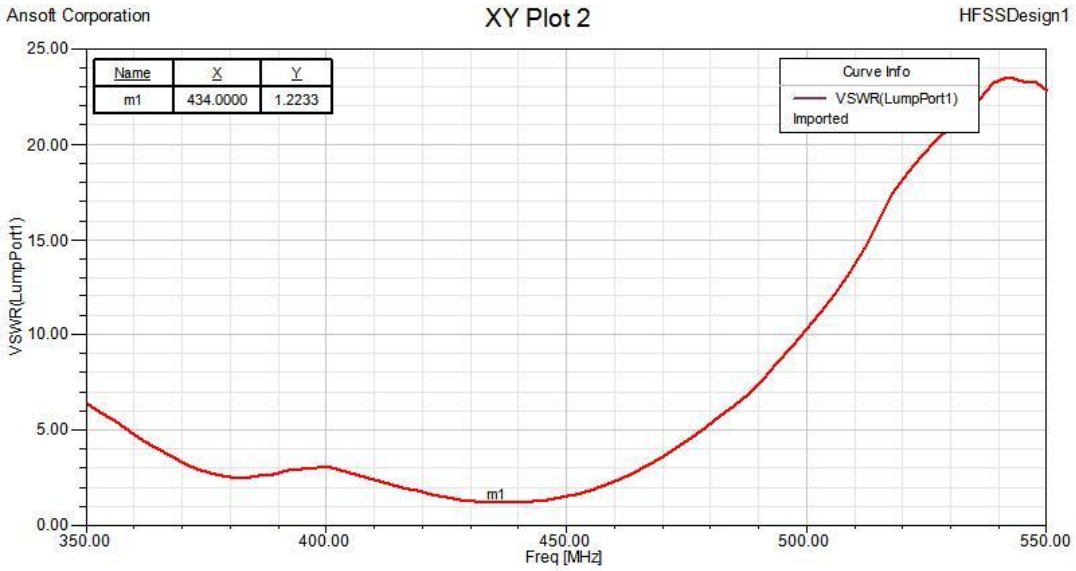

Figure 5.1.4: The first meander-line antenna Voltage Standing Wave Ratio (VSWR).

5.1.5 2D Radiation Pattern after Matching

Red: Co-polarization, Green: Cross-polarization

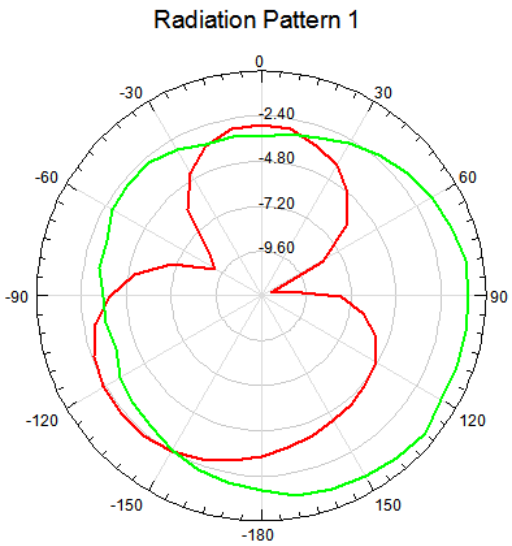

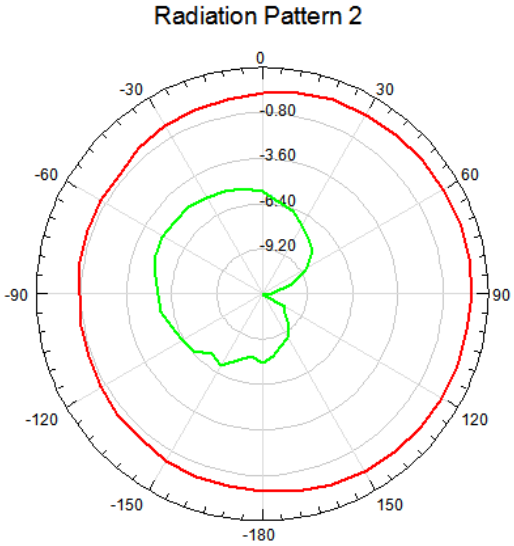

Figure 5.1.5: E-plane Co-cross polarization

Figure 5.1.6: H-plane Co-cross polarization

Unit: dBi		E-plane co-polarization	E-plane cross-polar.	H-plane co-polar.	H-plane cross-polar.
Board 1	Max.Gain	-2.25	-0.55	1.05	-4.9
	Min.Gain	-11.45	-3.75	-0.7	-12

Table 5.1.1 First meander-line antenna gain

5.2 The Second Meander-line Antenna

5.2.1 Antenna prototype and Matching Network

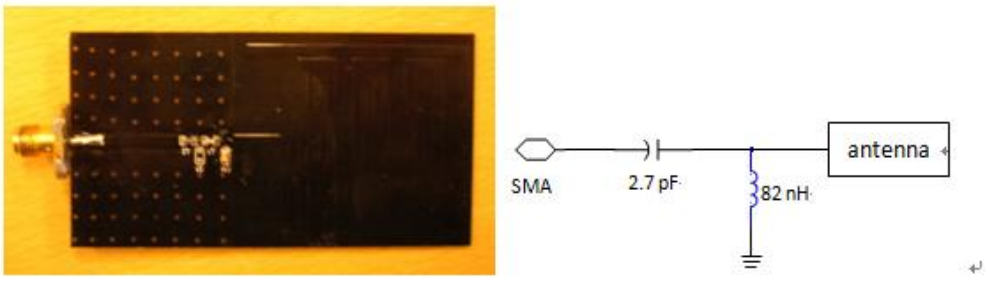

Figure 5.2.1: Second meander-line antenna prototype and matching network.

5.2.2 S11 Reflection Coefficient (dB) after Matching

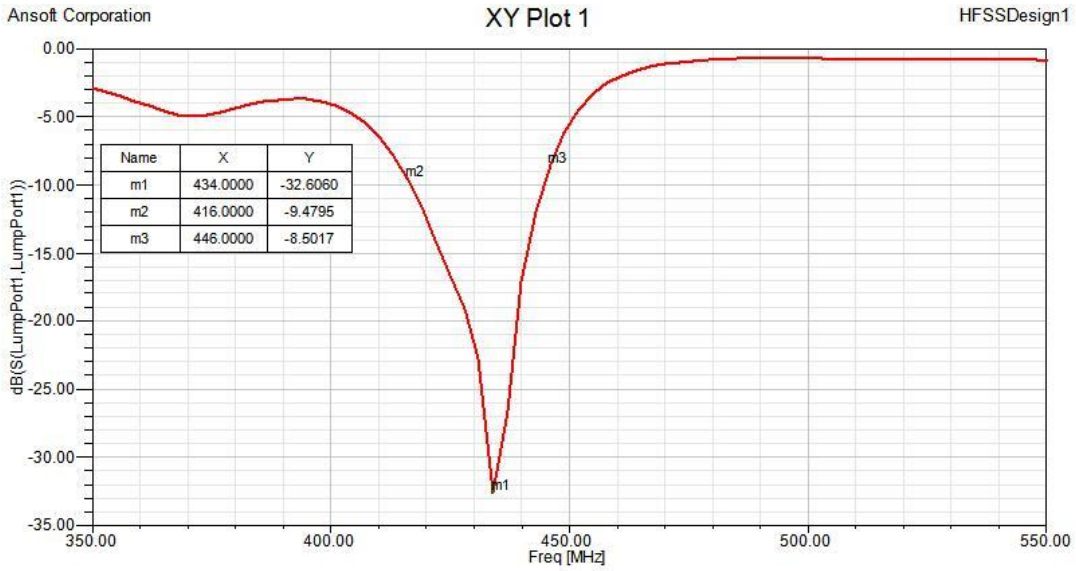

Figure 5.2.2: The second meander-line antenna input-port reflection coefficient (S11) expressed in dB.

5.2.3 Simulated Smith Chart

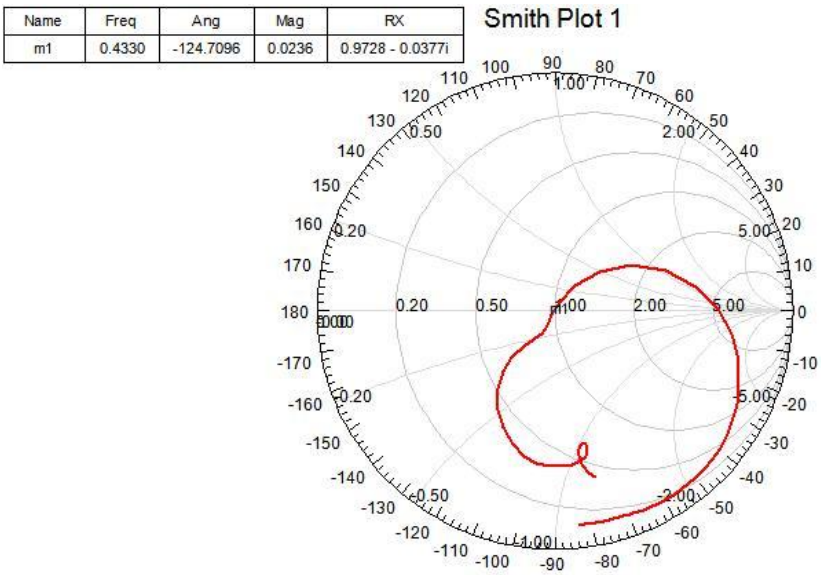

Figure 5.2.3: The second meander-line antenna input-port Smith Chart.

5.2.4 Voltage Standing Wave Ratio (VSWR) after matching

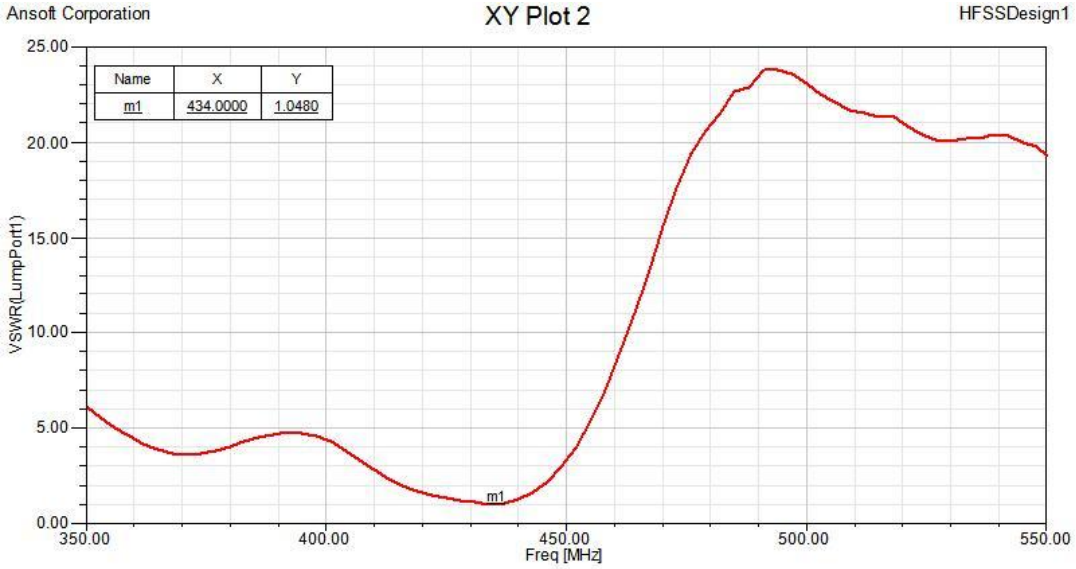

Figure 5.2.4: The second meander-line antenna input-port Voltage Standing Wave Ratio

5.2.5 2D Radiation Pattern after Matching

Red: Co-polarization, Green: Cross-polarization

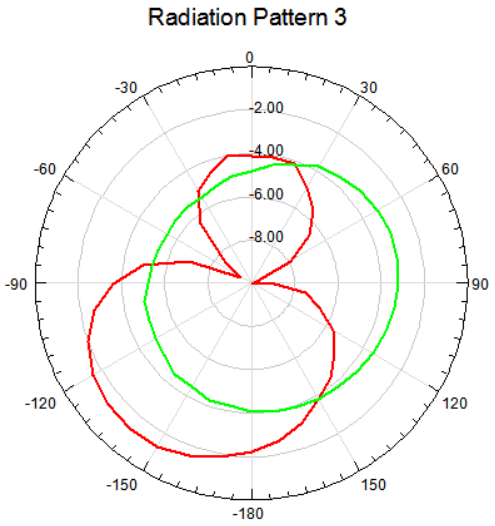

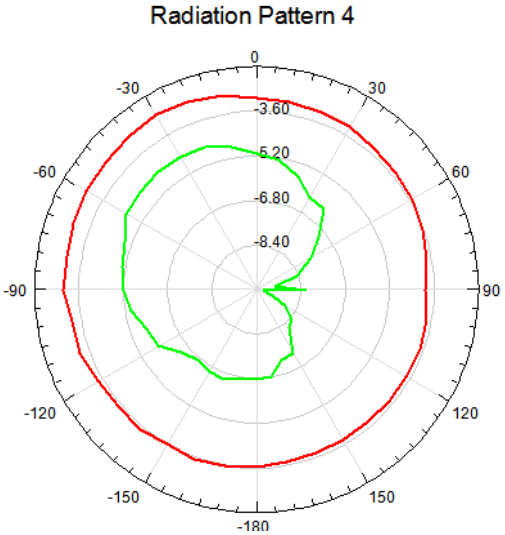

Figure 5.2.5: E-plane Co-cross polarization **Figure 5.2.6: H-plane Co-cross polarization**

Unit: dBi		E-plane co-polarization	E-plane cross-polar.	H-plane co-polar.	H-plane cross-polar.
Board 2	Max.Gain	-1.27	-3.26	-2.76	-4.46
	Min.Gain	-9.95	-5.51	-3.81	-9.76

Table 5.2.1 Second meander-line antenna gain

5.3 The Third Meander-line Antenna

5.3.1 Antenna prototype and matching network

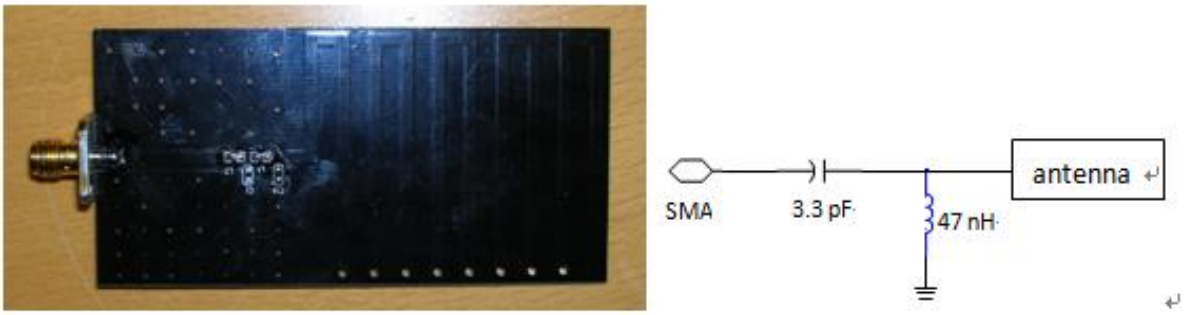

Figure 5.3.1: Third meander-line antenna prototype and matching network.

5.3.2 S11 Reflection Coefficient (dB) after Matching

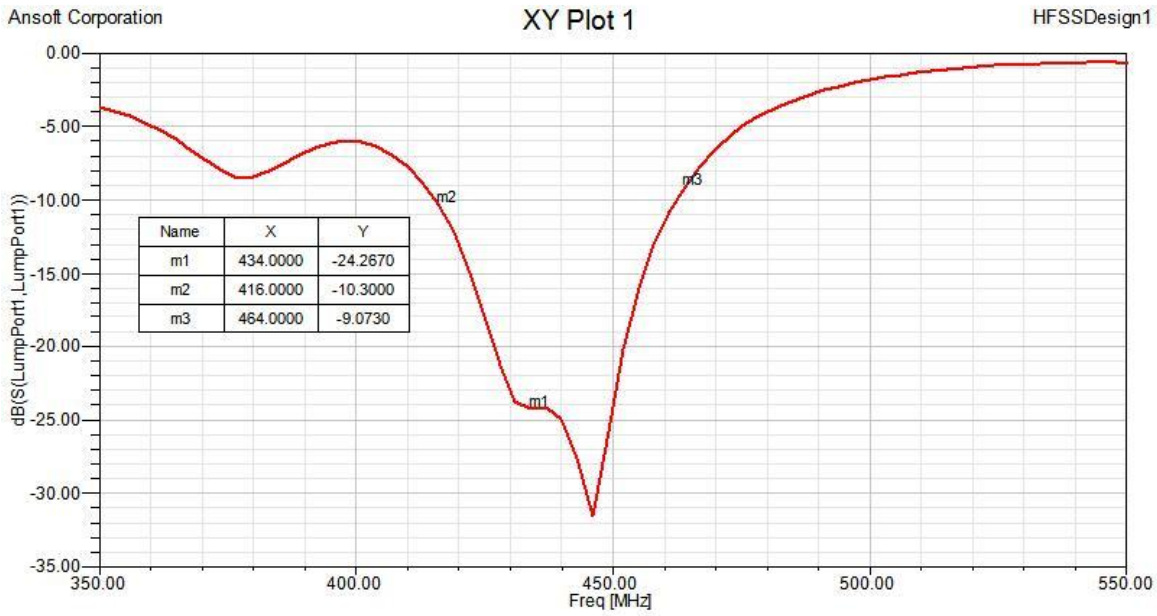

Figure 5.3.2: The third meander-line antenna input-port reflection coefficient (S11) expressed in dB.

5.3.3 Simulated Smith Chart

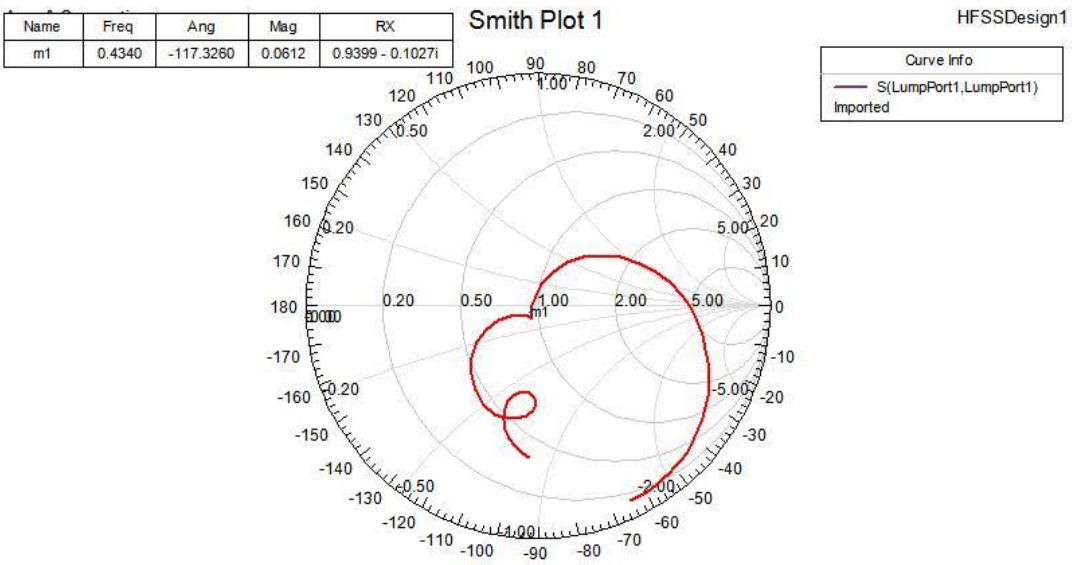

Figure 5.3.3: The third meander-line antenna input-port Smith Chart.

5.3.4 Voltage Standing Wave Ratio (VSWR) after matching

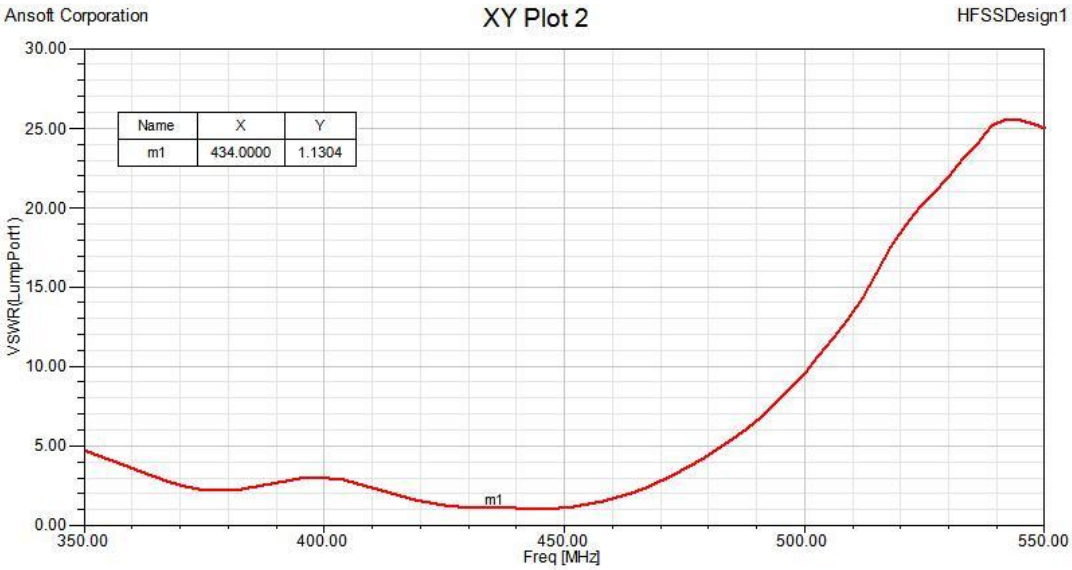

Figure 5.3.4: The third meander-line antenna input-port Voltage Standing Wave Ratio

5.3.5 2D Radiation Pattern after Matching

Red: Co-polarization, Green: Cross-polarization

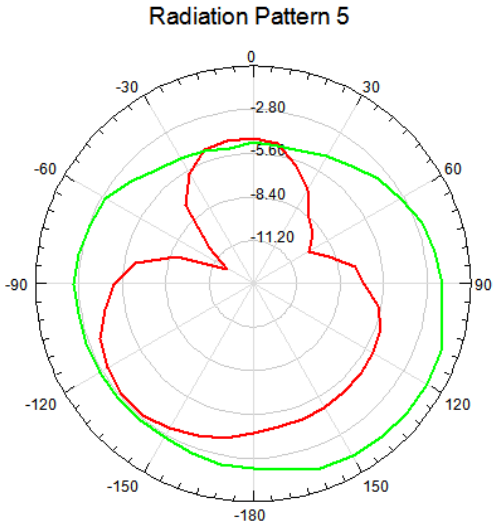

Figure 5.3.5: E-plane Co-cross polarization

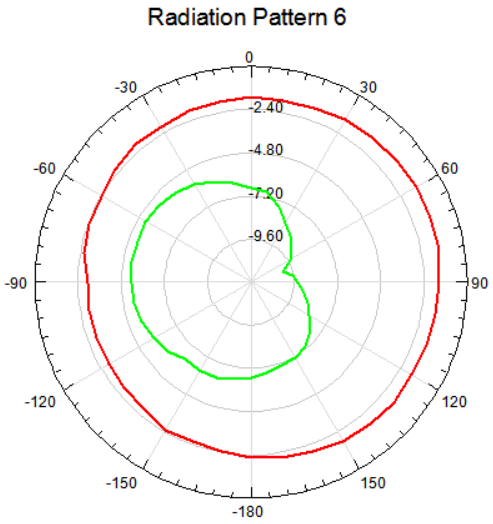

Figure 5.3.6: H-plane Co-cross polarization

Unit: dBi		E-plane co-polarization	E-plane cross-polar.	H-plane co-polar.	H-plane cross-polar.
Board 3	Max.Gain	-2.96	-1.06	-1.56	-5.26
	Min.Gain	-12.06	-5.15	-2.91	-10.11

Table 5.3.1 Third meander-line antenna gain

5.4 Measured Results

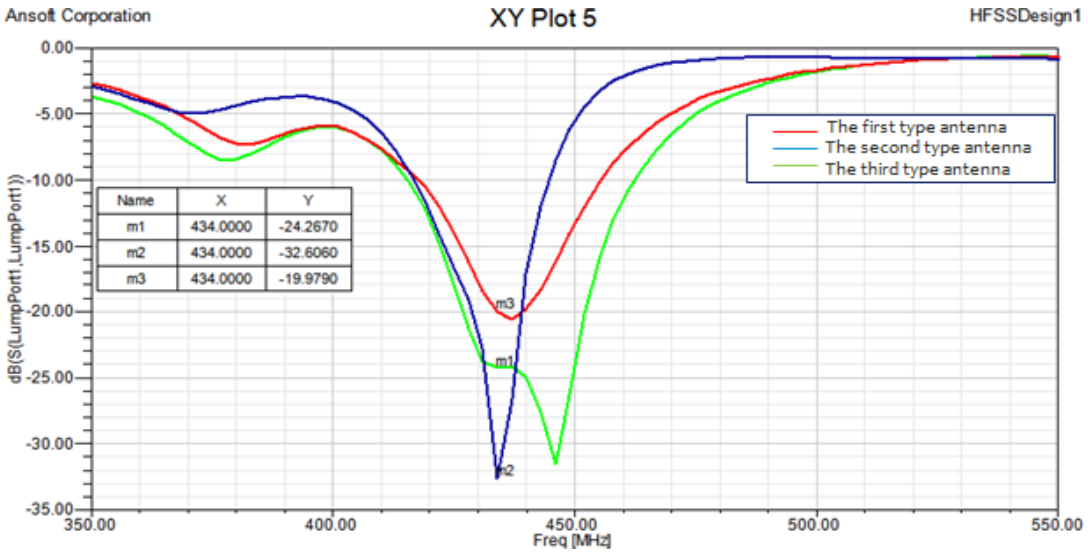

Fig 5.3.7 Comparison of three different antennas S parameter

According to [20], for omnidirectional antennas, directivity can be calculated using formula:

$$D_0 = \frac{101}{HPBW(\deg rees) - 0.0027[HPBW(\deg rees)]^2}$$

Then, according to the formula, Efficiency=Gain/Directivity, the efficiency of three PCB antennas are separately: 85.9%, 50% and 52.8%.

From the table 5.1.1, 5.2.1, 5.3.1, we can see that the peak gain of the three boards is separately 1.05 dBi, -1.27 dBi and -1.06 dBi. Base upon measured results as shown in table 5.4.1, S11 of three different antennas are shown in figure 5.3.7. Considering the performance of antenna, lower cost and operation bandwidth, the third meander-line antenna is the best one. The measured data is quite different from predicted with the simulation, such as S11 coefficient, radiation efficiency, operational bandwidth, and peak gain. The reasons are presented in conclusion Chapter 7.

Design	Bandwidth		Actual S11 Reflection Coefficient at 433MHz		Max Gain		Antenna efficiency	
	simulate	measure	simulate	measure	simulate	measure	simulate	Measure
Board1	10 MHz	39 MHz	-20.36 dB	-20dB	1 dBi	1.05 dBi	92%	85.9%
Board2	4 MHz	30 MHz	-24.67 dB	-32dB	-4 dBi	-1.27 dBi	39%	50%
Board3	5 MHz	42 MHz	-34.8 dB	-24db	0 dBi	-1.06 dBi	51%	53%

Table 5.4.1 Comparison of simulated and measured data

CHAPTER 6

Integrated Transceiver CC1101

6.1 Introduction

CC1101 is a low-cost sub-1 GHz transceiver designed for the very low-power wireless applications [21]. It provides extensive hardware support for packet handling, data buffering, burst transmissions, clear channel assessment, link quality indication and wake-on-radio [21]. In a typical system, the **CC1101** will be used together with a microcontroller and a few additional passive components. [21] The **CC1101** pin-out is shown clearly in Figure 6.1.1.

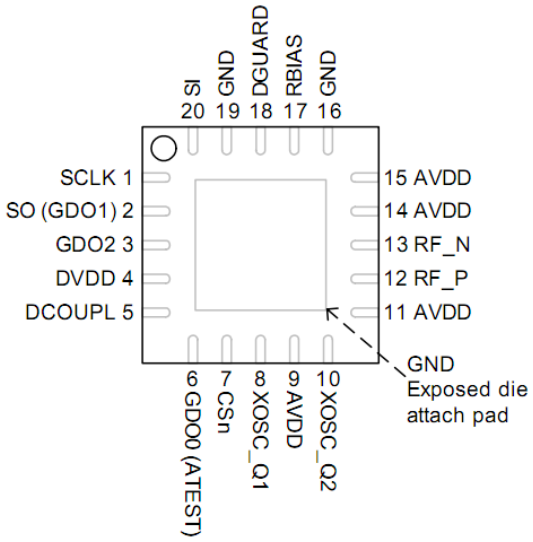

Figure 6.1.1: Top View of the Pin out [21].

6.2 Balun Matching Network

In our work, the designed antenna is single ended antennas, which is also called unbalanced antenna. However, the output impedance seen from the RF-port to CC1101 is equal to 116 - 41j. In order to obtain the maximum power transferred, the impedance seen from the RF-port towards the antenna is 116 + 41j. Therefore, a balanced-to-unbalanced matching network is required to optimize power transfer from the CC1101 transceiver to the antenna load. In our case, a balun is used to transfer the impedance to 50 Ohm which is the same as the input impedance of a matched antenna. A Balun can be shown clearly in figure 6.2.1.

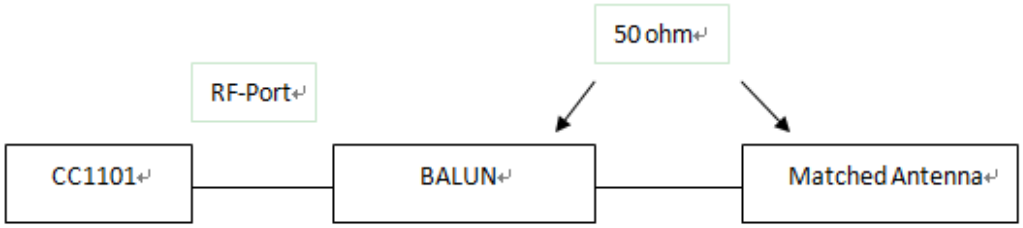

Figure 6.2.1: The exact location of a Balun.

6.3 Application

CC1101 is mainly applied in the ultra low-power wireless fields which operate in the 315/433/868/915 MHz ISM/SRD bands. Also, it is applied in wireless alarm and security systems. In the aspect of industrial monitoring and control, **CC1101** also plays an important part. The typical application and evaluation circuit at 433 MHz are shown in Figure 6.3.1 and the function of every component of this circuit is described in table 6.3-1. The reference circuit Bill of Materials (BOM) can be found in table 6.3-2.

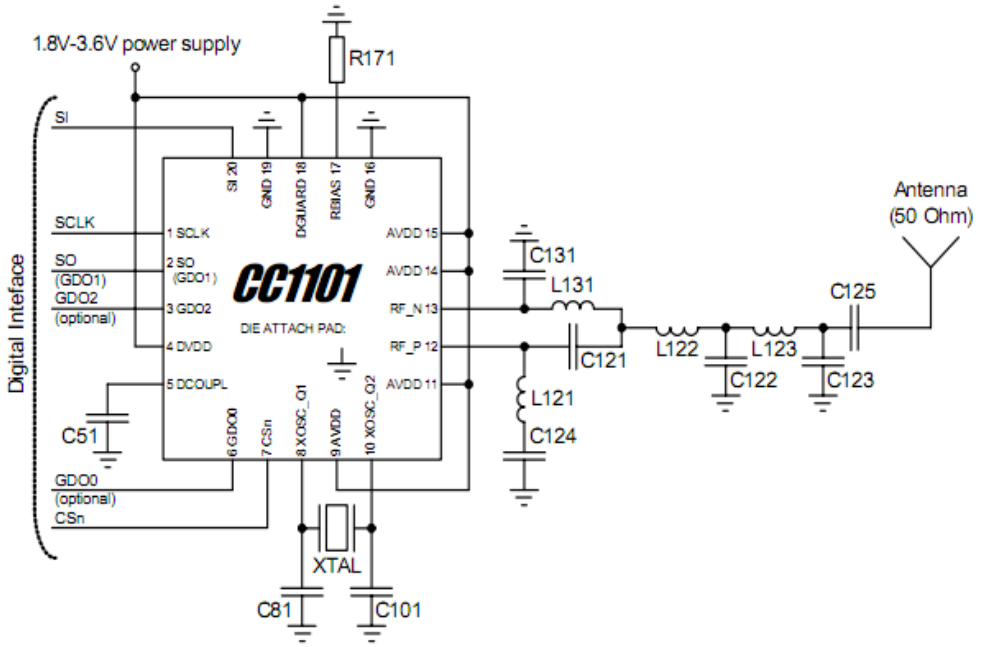

Figure 6.3.1: Schematic of application Circuit at 433 MHz [21]

Component	Description
C51	Decoupling capacitor for on-chip voltage regulator to digital part
C81/C101	Crystal loading capacitors
C121/C131	RF balun/matching capacitors
C122	RF LC filter/matching filter capacitor (315 and 433 MHz). RF balun/matching capacitor (868/915 MHz).
C123	RF LC filter/matching capacitor
C124	RF balun DC blocking capacitor
C125	RF LC filter DC blocking capacitor and part of optional RF LC filter (868/915 MHz)
C126	Part of optional RF LC filter and DC-block (868/915 MHz)
L121/L131	RF balun/matching inductors (inexpensive multi-layer type)
L122	RF LC filter/matching filter inductor (315 and 433 MHz). RF balun/matching inductor (868/915 MHz). (inexpensive multi-layer type)
L123	RF LC filter/matching filter inductor (inexpensive multi-layer type)
L124	RF LC filter/matching filter inductor (inexpensive multi-layer type)
L125	Optional RF LC filter/matching filter inductor (inexpensive multi-layer type) (868/915 MHz)
L132	RF balun/matching inductor. (inexpensive multi-layer type)
R171	Resistor for internal bias current reference
XTAL	26MHz - 27MHz crystal

Table 6.3-1: List of External Components [21].

Component	Value at 315MHz	Value at 433MHz	Value at 868/915MHz	Manufacturer
C51	100 nF ± 10%, 0402 X5R			Murata GRM1555C series
C81	27 pF ± 5%, 0402 NP0			Murata GRM1555C series
C101	27 pF ± 5%, 0402 NP0			Murata GRM1555C series
C121	6.8 pF ± 0.5 pF, 0402 NP0	3.9 pF ± 0.25 pF, 0402 NP0	1.0 pF ± 0.25 pF, 0402 NP0	Murata GRM1555C series
C122	12 pF ± 5%, 0402 NP0	8.2 pF ± 0.5 pF, 0402 NP0	1.5 pF ± 0.25 pF, 0402 NP0	Murata GRM1555C series
C123	6.8 pF ± 0.5 pF, 0402 NP0	5.6 pF ± 0.5 pF, 0402 NP0	3.3 pF ± 0.25 pF, 0402 NP0	Murata GRM1555C series
C124	220 pF ± 5%, 0402 NP0	220 pF ± 5%, 0402 NP0	100 pF ± 5%, 0402 NP0	Murata GRM1555C series
C125	220 pF ± 5%, 0402 NP0	220 pF ± 5%, 0402 NP0	100 pF ± 5%, 0402 NP0 or 12 pF ± 5%, 0402 NP0 when part of optional filter	Murata GRM1555C series
C126			47 pF ± 5%, 0402 NP0	Murata GRM1555C series
C131	6.8 pF ± 0.5 pF, 0402 NP0	3.9 pF ± 0.25 pF, 0402 NP0	1.5 pF ± 0.25 pF, 0402 NP0	Murata GRM1555C series
L121	33 nH ± 5%, 0402 monolithic	27 nH ± 5%, 0402 monolithic	12 nH ± 5%, 0402 monolithic	Murata LQG15HS series
L122	18 nH ± 5%, 0402 monolithic	22 nH ± 5%, 0402 monolithic	18 nH ± 5%, 0402 monolithic	Murata LQG15HS series
L123	33 nH ± 5%, 0402 monolithic	27 nH ± 5%, 0402 monolithic	12 nH ± 5%, 0402 monolithic	Murata LQG15HS series
L124			12 nH ± 5%, 0402 monolithic	Murata LQG15HS series
L125			3.3 nH ± 5%, 0402 monolithic	Murata LQG15HS series
L131	33 nH ± 5%, 0402 monolithic	27 nH ± 5%, 0402 monolithic	12 nH ± 5%, 0402 monolithic	Murata LQG15HS series
L132			18 nH ± 5%, 0402 monolithic	Murata LQG15HS series
R171	56 kΩ ± 1%, 0402	Koa RK73 series		
XTAL	26.0 MHz surface mount crystal			NDK, AT-41CD2

Table 6.3-2: List of Materials for the Application Circuit [21].

6.4 PCB layout of the antenna with CC1101

After knowing the function of CC1101, we can make the drawing of the Printed Circuit Board (PCB) with the CC1101, application circuits and the matched antenna. Before the final layout of our design, we draw the schematic using PADS 9.0. It is shown in Figure 6.4.1.

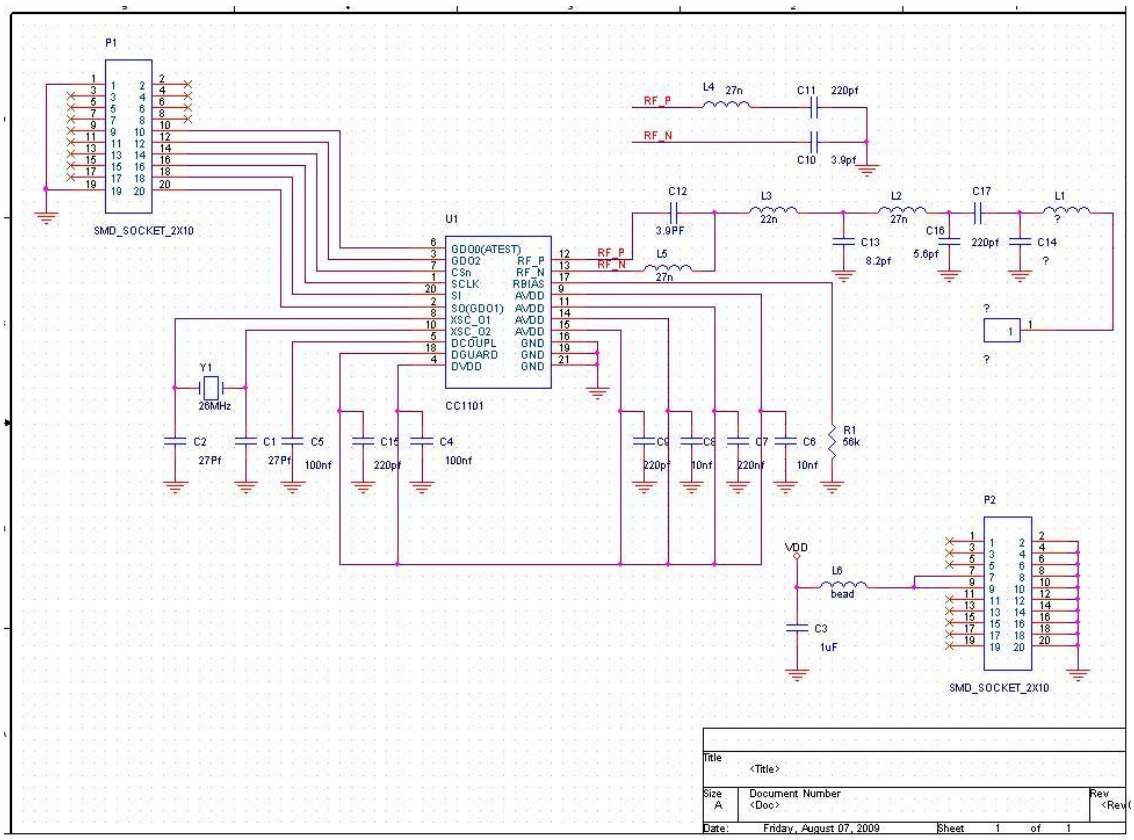

Figure 6.4.1 Schematic of the design including CC1101 and Antenna.

After drawing of the schematic, the layout of passive components and socket are made, which are shown in Figure 6.4.2 and Figure 6.4.3.Then we can utilize the PADS Layout function supplied by PADS 9.0 to make our final PCB layout which is shown in Figure 6.4.4. Finally, from the Gerber file, the PCB professional factory can make the completed prototype which can be seen in Figure 6.4.5.

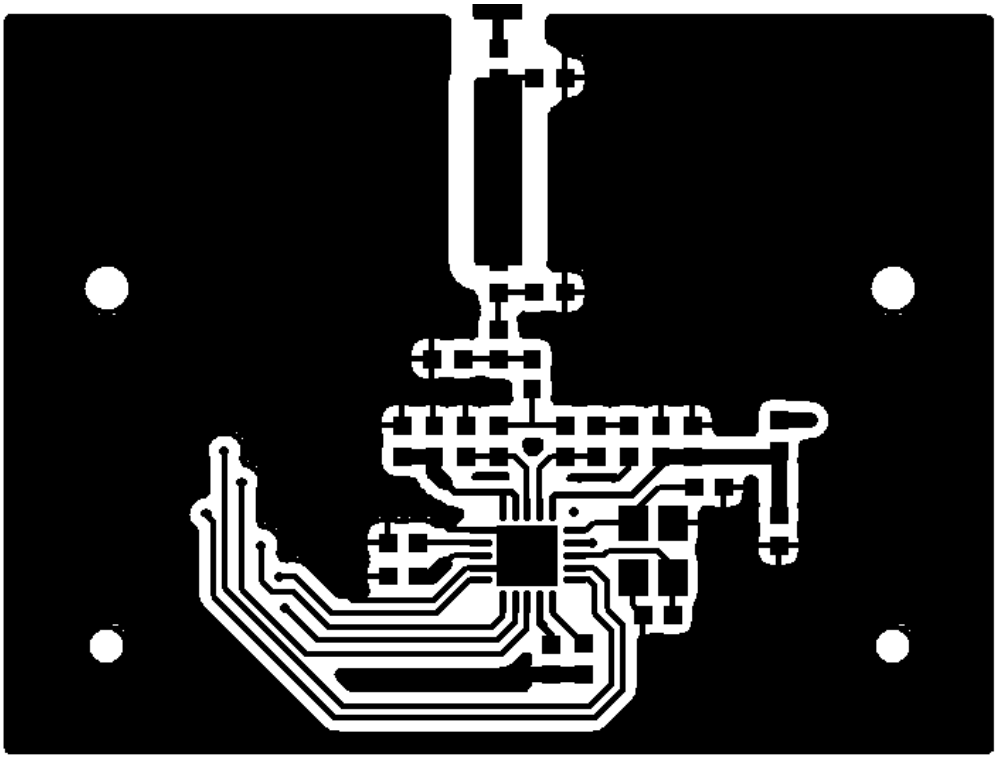

Figure 6.4.2: Layout of CC1101, its application circuit and matching network.

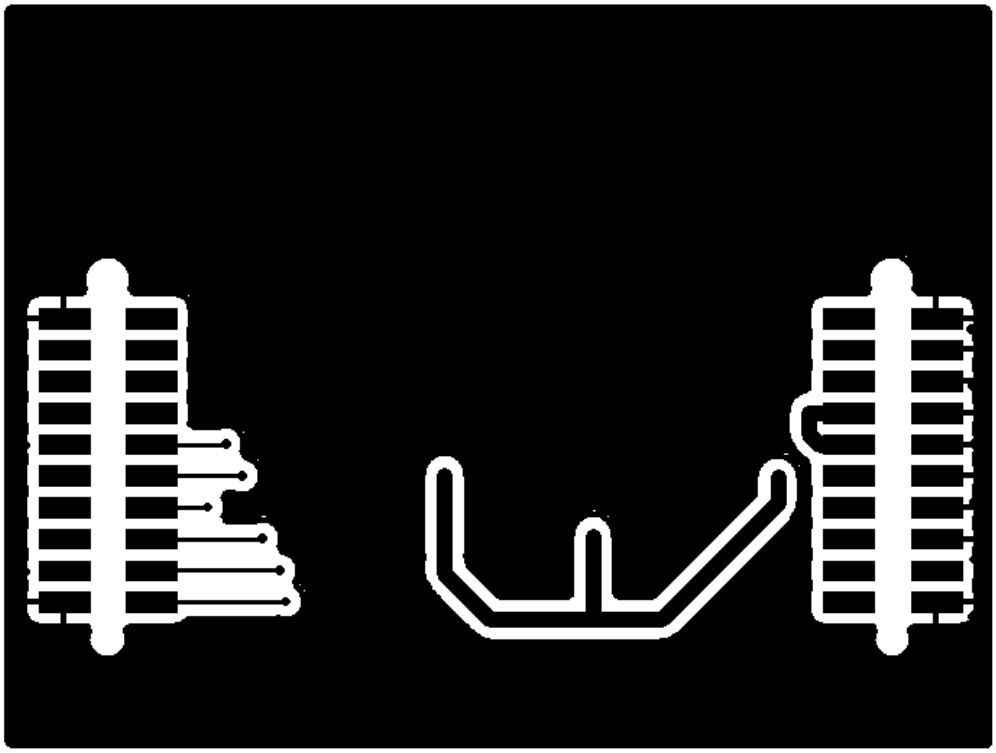

Figure 6.4.3: Layout of Sockets.

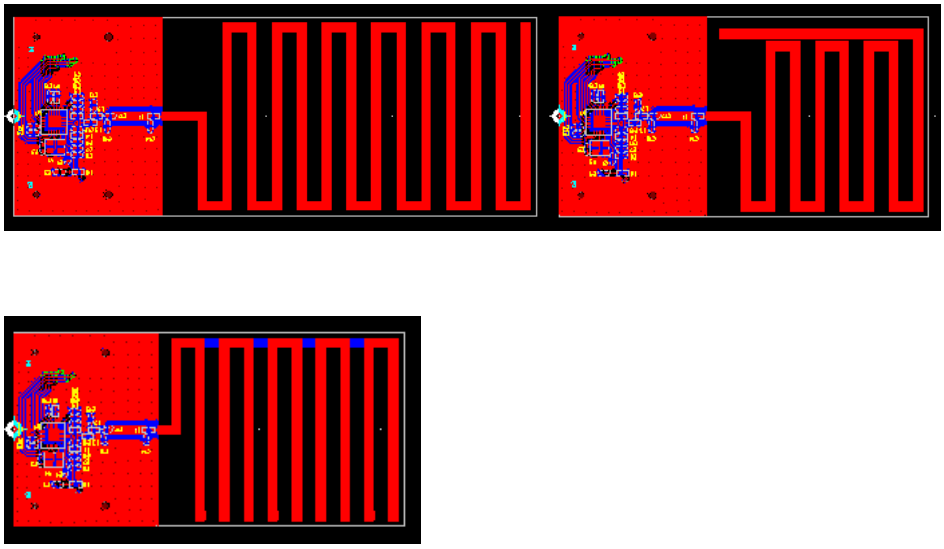

Figure 6.4.4: Final PCB Layout Using PADS 9.0.

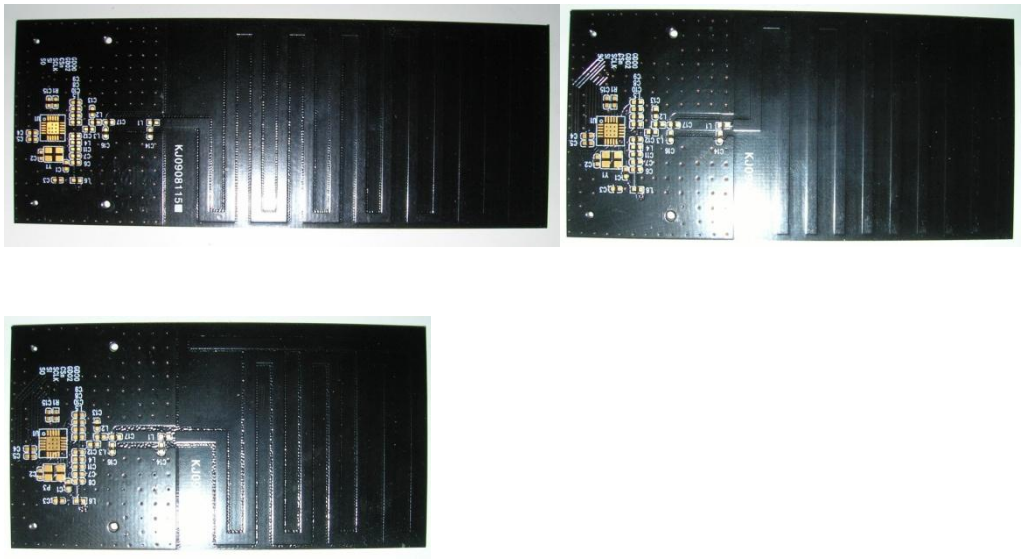

Figure 6.4.5: Completed Prototype of Antenna with CC1101.

CHAPTER 7

CONCLUSIONS

The actual measurement data is better than the simulation. There are many reasons which make the measurement data different from predicted with the simulation. The reason is the board thickness and copper thickness; they are lower thickness than simulation when the board is manufacture. And the main reason is that the ground will affect the antenna S parameters. As we know that the wave resonates only between the antenna and the ground of microstrip. When we measure the antenna in the Anechoic Chamber, the antenna must be fixed on the column and the column is like ground. It results in the difference.

In this project the two-sided printing meander-line antenna and an integrated transceiver circuit are presented. At the beginning of this project, we introduce the development of antenna and it confront with some problems. According to the previous work, the printed antenna is either high efficiency or small size which is introduced in background part .In the objective part introduces the primary goal of this project is to improve the dimension of antenna and the radiation efficiency according to the research meander line antenna model and coupling element technology can solve some problems. In Chapter 2, we introduce antenna basic theory meander line antenna principle of work and characteristic of coupling element, studying and analysis what is the relationship between size efficiency and antenna gain, and how to use the coping element to reduce the size of antenna and increase the radiation efficiency and use inductor and capacitor to matching network. After that bring up three meander-line antennas with different constructions base upon simulation and measurement, new method of meander-line antenna is developed. Last describe principle of Integrated Transceiver CC1101, after knowing the function of CC1101, Printed Circuit Board (PCB) with the CC1101, application circuits and the matched antenna are designed and manufactured.

There are some specific reasons which limit this research such as fixed substrate material and the fixed thickness of board. In the future work, different PCB substrate material and thin board can be performance to reduce the size of antenna, also power amplifier can be considered to add in the integrated circuit part to improve the transmission performance.

Reference

[1] K. Finkenzeller, "*RFID Handbook*", John Wiley & Son, England, 1999.

[2] Gaetano Marrocco, Alessandro Fonte and Fernando Bardati, "Evolutionary Design of Miniaturized Meander-Line Antennas for RFID Applications",DISP, University of Tor Vergata – Via di Tor Vergata, 110, 00133 Roma, ITALY.

[3] G.A.Mavridis, D.E.Anagnostou, C.G.Christodoulou, and M.T.Chryssomallis "Quality factor Q of a miniaturized meander microstrip patch antenna", IEEE Trans. Antennas Propagat, pp.1-4, July 2008.

[4] S.Reed, L.Desclos, C.Terrt, S.Toutain, "Size reduction of a patch antenna by means of inductive loads", Microwave and Optical Technology Letters, Wiley Periodicals, Inc. Vol 29, pp.79 – 81, 27th Feb 2001.

[5] L.Desclos, Y.Mahe, S.Reed, G.Poilasne, S.Toutain, "Patch Antenna size reduction by combining inductive loading and short-points", Microwave and Optical Technology Letters, Wiley Periodicals Inc, Vol.30, pp.385 – 386, 15th Aug 2001.

[6] S.VILLERS, "Patch antenna with reduced size for 400MHz transmission in confined surroundings", IEEE Trans. Antennas Propagat, pp.1-4, Nov.2006.

[7] J.Rashed, C. Tai, "A new class of resonant antennas", IEEE Trans. Antennas Propagat., Vol.39, N.9, pp.1428-1430, 1991.

[8] G.Leon, R.R. Boix, F. Medina, "A comparison among different reduced-size resonant microstrip patch", Microwave and Optical Tech. Letters, Vol.29, No.3, pp.143-146, 2001.

[9] Vincent F. Fusco, "Foundations of Antenna Theory and Techniques", Malaysia, Pearson Education Limited, 2005.

[10] Takashi Yamano, Jun Itoh, Kim Yongho, "Fundamental Characteristics of Planar Folded Dipole Antenna with a Feed Line", IEEE International Symposium on Antennas & Propagation and USNC/URSI Meeting, July 2008.

[11] J.R. James, P.S. Hall, "Handbook of Microstrip Antennas", London, Peter Peregrinus Ltd, Vol. 1, 1989.

[12] Auden Andersen, “Antenna Select for Low Power Wireless Application”, China, EDN magazine, Dec 2008, pp.25-27.

[13] Pozar, David M. Microwave Engineering, Third Edition. Sussex, England: John Wiley and Sons, Inc., pp. 143-149, 155-156，223-224, 2005.

[14] Matthew Loy and Iboun Sylla, “Fundamentals of ISM-Band and short range device antennas”, application report SWRA046A,Texas Instruments.pp.10, August 2005.

[15] Louis E. Frenzel, Louis E, “Printed-Circuit-Board Antennas”, Frenzel, pp.1-2, March 31, 2005

[16] Zhixin Huang, “Application of an Inductor Model to Design and Analysis of Printed Meander Line Antennas”, Taiwan, China, pp.10-12, July 2007.

[17] Randy Bancroft, “Fundamental Dimension Limits of Antennas”, Centruion Wireless Technologies, Westminster, Colorado, USA, pp. 8-10.

[18] Chen, Zhi Ning. **“**Antennas for Portable Devices”, Sussex, England: John Wiley and Sons Ltd., 2007.pp. 20-21.

[19] Waterhouse, Rod, **“**Printed Antennas for Wireless Communications”, Sussex, England: John Wiley and Sons Ltd, 2007.pp. 183-184, 258.

[20] C.A.Balanis. “Antenna Theory Analysis and Design” New York: John Wiley&Sons Ltd., 1997.pp.1, 28, 723.

[21] Associated Author. CC1101 Datasheet: Low Power Sub-1 GHz RF Transceiver. www.ti.com. [Online] 5th, May 2009. [Cited: Nov 18th, 2009.]